

Probing isospin- and momentum-dependent nuclear effective interactions in neutron-rich matter

Lie-Wen Chen^{1,2}, Che Ming Ko³, Bao-An Li^{4,5}, Chang Xu⁶, and Jun Xu⁷

¹ Department of Physics and Astronomy and Shanghai Key Laboratory for Particle Physics and Cosmology, Shanghai Jiao Tong University, Shanghai 200240, China

² Center of Theoretical Nuclear Physics, National Laboratory of Heavy Ion Accelerator, Lanzhou 730000, China

³ Cyclotron Institute and Department of Physics and Astronomy, Texas A&M University, College Station, TX 77843-3366, USA

⁴ Department of Physics and Astronomy, Texas A&M University-Commerce, Commerce, TX 75429-3011, USA

⁵ Department of Applied Physics, Xi'an Jiao Tong University, Xi'an 710049, China

⁶ Department of Physics, Nanjing University, Nanjing 210008, China

⁷ Shanghai Institute of Applied Physics, Chinese Academy of Sciences, Shanghai 201800, China

Received: date / Revised version: date

Abstract. The single-particle potentials for nucleons and hyperons in neutron-rich matter generally depends on the density and isospin asymmetry of the medium as well as the momentum and isospin of the particle. It further depends on the temperature of the matter if the latter is in thermal equilibrium. We review here the extension of a Gogny-type isospin- and momentum-dependent interaction in several aspects made in recent years and their applications in studying intermediate-energy heavy ion collisions, thermal properties of asymmetric nuclear matter and properties of neutron stars. The importance of the isospin- and momentum-dependence of the single-particle potential, especially the momentum dependence of the isovector potential, is clearly revealed throughout these studies.

PACS. 21.65.Ef Symmetry energy – 21.30.Fe Forces in hadronic systems and effective interactions – 25.70.-z Low and intermediate energy heavy-ion reactions – 26.60.-c Nuclear matter aspects of neutron stars – 97.60.Jd Neutron stars

1 Introduction

One of the fundamental questions in contemporary nuclear physics and astrophysics is to understand quantitatively the in-medium nuclear effective interactions, which are directly related to the structure and decay properties of finite nuclei, the reaction dynamics induced by nuclei, the equation of state (EOS) of dense nuclear matter, the properties of compact stars, and the explosion mechanism of supernova [1, 2, 3, 4, 5, 6, 7, 8]. The in-medium nuclear effective interactions generally depend on the medium baryon density and isospin asymmetry, the particle momentum, and the particle isospin. Theoretically, information on the in-medium nuclear effective interactions usually can be extracted from various approaches using the microscopic many-body theory, the effective-field theory, and phenomenological models. In the microscopic many-body theory approach [9, 10, 11, 12, 13, 14, 15, 16, 17, 18, 19], vacuum bare nucleon-nucleon (NN) interactions, that are fitted to high-precision experimental data, are used to describe the nuclear system, and the resulting in-medium nuclear effective interactions (G-matrix) are therefore free of parameters. In the effective-field theory (EFT) approach [20, 21, 22], effective nuclear interactions are constructed from low energy QCD

and its symmetry breaking, and thus they usually have a smaller number of free parameters and a correspondingly higher predictive power. In the phenomenological approach [23, 24, 25, 26, 27, 28, 29, 30, 31, 32, 33, 34, 35, 36, 37, 38, 39, 40, 41], the nuclear many-body problem is generally treated using effective density- (momentum- and isospin-) dependent nuclear forces or effective interaction Lagrangians with parameters adjusted to fit the properties of a number of finite nuclei and/or nuclear scattering data. Although a lot of useful information on the in-medium nuclear effective interactions around normal nuclear density with relatively small isospin asymmetry has been obtained by analyzing experimental data based on these various approaches, corresponding knowledge at high baryon density and/or large isospin asymmetry remains very limited.

Indeed, both the EFT and phenomenological approaches usually give excellent descriptions of the nuclear matter properties around or below the saturation density with relatively small isospin asymmetry. Their predictions on properties of nuclear matter at the high density region and/or large isospin asymmetry are, however, likely unreliable. In addition, due to different approximations or techniques adopted in various microscopic many-body the-

ory approaches, their predictions on the properties of nuclear matter and the in-medium nuclear effective interactions could be very different even for the same vacuum bare NN interaction [42,43]. In particular, predictions on the isovector properties of nuclear matter, especially the density dependence of the nuclear symmetry energy, are still largely different in different microscopic many-body theory approaches or the same microscopic many-body theory approach but with different vacuum bare NN interactions [43]. Therefore, the experimental information on the in-medium nuclear effective interactions and properties of nuclear matter at extremely large isospin and high baryon density is of critical importance, and this provides a strong motivation for studying isospin-dependent phenomena with radioactive nuclei at the new/planning rare isotope beam facilities around the world, such as CSR/Lanzhou and BRIF-II/Beijing in China, RIBF/RIKEN in Japan, SPIRAL2/GANIL in France, FAIR/GSI in Germany, SPES/LNL in Italy, RAON in Korea, and FRIB/NSCL and T-REX/TAMU in USA.

In the present contribution, we review the isospin- and momentum-dependent MDI interaction, which has been extensively used in recent years to study heavy ion collisions induced by neutron-rich nuclei, the thermal properties of asymmetric nuclear matter including its liquid-gas phase transition, and the properties of neutron stars. We also review the extended MDI interaction for the baryon octet and its application to hybrid stars as well as the improved MDI interaction with separate density dependence for neutrons and protons which takes into account more accurately the effect of the isospin dependence of in-medium NN interactions. We further highlight some results from these studies with emphasis on the effects of the momentum dependence of nuclear mean-field potential, especially its isovector symmetry potential in asymmetric nuclear matter. These studies demonstrate the importance of both the isospin and momentum dependence of nuclear mean-field potential in asymmetric nuclear matter, and provide useful information on the isospin- and momentum-dependent effective interactions in such a matter.

This article is organized as follows. In Section 2, we briefly introduce the nuclear symmetry energy and the nuclear symmetry potential. Section 3 gives some details of the isospin- and momentum-dependent MDI interaction. We then highlight some applications of the MDI interaction in Section 4. In Section 5, the extended MDI interaction for the baryon octet and the improved MDI interaction with separate density dependence for neutrons and protons are reviewed. Finally, a summary is presented in Sections 6.

2 The symmetry energy and the symmetry potential

For completeness, we include in the following a brief introduction to the nuclear symmetry energy and the nuclear symmetry potential as both are closely linked to the isovector properties of asymmetric nuclear matter. While

there are extensive discussions in the literature on the symmetry energy, relatively little attention has been paid to the equally important symmetry potential.

2.1 Nuclear symmetry energy

The binding energy per nucleon of an isospin asymmetric nuclear matter with neutron density ρ_n and proton density ρ_p , i.e., the EOS of the asymmetric nuclear matter can be generally expressed as a power series in the isospin asymmetry $\delta = (\rho_n - \rho_p)/\rho$ ($\rho = \rho_n + \rho_p$ is the total nucleon density). To the 2nd-order in δ , it can be expressed as

$$E(\rho, \delta) = E_0(\rho) + E_{\text{sym}}(\rho)\delta^2 + O(\delta^4), \quad (1)$$

where $E_0(\rho) = E(\rho, \delta = 0)$ is the binding energy per nucleon of symmetric nuclear matter, and

$$E_{\text{sym}}(\rho) = \frac{1}{2!} \frac{\partial^2 E(\rho, \delta)}{\partial \delta^2} \Big|_{\delta=0} \quad (2)$$

is the nuclear symmetry energy. The absence of odd-order terms in δ in Eq. (1) is due to the neutron-proton exchange symmetry in nuclear matter when the Coulomb interaction is neglected and the charge symmetry of nuclear forces is assumed. Empirically, the coefficients of higher-order terms in δ are found to be negligible, e.g., the magnitude of the coefficient of δ^4 term at ρ_0 is estimated to be smaller than 1 MeV [10,11,18,44], compared to ~ 30 MeV for the coefficient of δ^2 term. Neglecting the contribution from higher-order δ terms in Eq. (1) corresponds to the well-known empirical parabolic law for the EOS of asymmetric nuclear matter, which has been verified by all many-body theory calculations at least for densities up to moderate values [8]. The density-dependent symmetry energy $E_{\text{sym}}(\rho)$ can thus be extracted approximately from

$$E_{\text{sym}}(\rho) \approx E(\rho, \delta = 1) - E(\rho, \delta = 0). \quad (3)$$

In this sense, the nuclear symmetry energy gives an estimation of the binding energy difference between pure neutron matter and symmetric nuclear matter. It should be noted that the possible presence of higher-order δ terms at supra-saturation densities can significantly modify the proton fraction in β -equilibrium neutron-star matter as well as the critical density for the direct Urca process that causes the faster cooling of neutron stars [44,45,46]. In addition, the higher-order δ terms have been shown to be very important in determining the core-crust transition density and pressure in neutron stars [44,47,48].

The binding energy per nucleon in symmetric nuclear matter $E_0(\rho)$ can be expanded around the saturation density ρ_0 as

$$E_0(\rho) = E_0(\rho_0) + \frac{K_0}{2!} \chi^2 + O(\chi^3), \quad (4)$$

where $\chi = (\rho - \rho_0)/3\rho_0$ is a dimensionless variable characterizing the deviations of the density from ρ_0 . The $E_0(\rho_0)$ on the right-hand-side of Eq. (4) is the binding energy

per nucleon in symmetric nuclear matter at its saturation density, and the coefficient

$$K_0 = 9\rho_0^2 \frac{d^2 E_0(\rho)}{d\rho^2} \Big|_{\rho=\rho_0}, \quad (5)$$

is the well-known incompressibility coefficient of symmetric nuclear matter characterizing the curvature of $E_0(\rho)$ at ρ_0 . Equation (4) represents the parabolic approximation to the EOS of symmetric nuclear matter. According to the definition of the saturation density ρ_0 , there is obviously no linear χ term in Eq. (4).

Similarly, the nuclear symmetry energy $E_{\text{sym}}(\rho)$ can also be expanded around ρ_0 as

$$E_{\text{sym}}(\rho) = E_{\text{sym}}(\rho_0) + L\chi + \frac{K_{\text{sym}}}{2!}\chi^2 + O(\chi^3), \quad (6)$$

where L and K_{sym} are, respectively, the slope and curvature parameters of the nuclear symmetry energy at ρ_0 , i.e.,

$$L = 3\rho_0 \frac{dE_{\text{sym}}(\rho)}{d\rho} \Big|_{\rho=\rho_0}, \quad (7)$$

$$K_{\text{sym}} = 9\rho_0^2 \frac{d^2 E_{\text{sym}}(\rho)}{d^2 \rho} \Big|_{\rho=\rho_0}. \quad (8)$$

The L and K_{sym} characterize the density dependence of the nuclear symmetry energy around the saturation density ρ_0 , and carry important information on both high and low density behaviors of the nuclear symmetry energy [49].

More generally, one can expand the $E_{\text{sym}}(\rho)$ around an arbitrary reference density ρ_r as

$$E_{\text{sym}}(\rho) = E_{\text{sym}}(\rho_r) + L(\rho_r)\chi_r + \frac{K_{\text{sym}}(\rho_r)}{2!}\chi_r^2 + O(\chi_r^3), \quad (9)$$

with $\chi_r = (\rho - \rho_r)/3\rho_r$, and the slope and curvature parameters of the nuclear symmetry energy at ρ_r are then defined, respectively, as

$$L(\rho_r) = 3\rho_r \frac{dE_{\text{sym}}(\rho)}{d\rho} \Big|_{\rho=\rho_r}, \quad (10)$$

$$K_{\text{sym}}(\rho_r) = 9\rho_r^2 \frac{d^2 E_{\text{sym}}(\rho)}{d^2 \rho} \Big|_{\rho=\rho_r}. \quad (11)$$

Since different observables may probe different density regions of the symmetry energy, the expansion in Eq. (9) could be very useful in some cases [50].

2.2 Nuclear symmetry potential

The single-nucleon potential $U_\tau(\rho, \delta, k)$ (we take isospin index $\tau = 1$ for neutrons and -1 for protons if not otherwise stated) in asymmetric nuclear matter generally depends on the nuclear matter density ρ , the nuclear matter isospin asymmetry δ , and the magnitude of the nucleon momentum k . Because of the isospin symmetry of nuclear interactions under the exchange of neutrons and

protons, the $U_\tau(\rho, \delta, k)$ can be expanded as a power series of δ as [51, 52]

$$\begin{aligned} U_\tau(\rho, \delta, k) &= U_0(\rho, k) + \sum_{i=1,2,\dots} U_{\text{sym},i}(\rho, k)(\tau\delta)^i \\ &= U_0(\rho, k) + U_{\text{sym},1}(\rho, k)(\tau\delta) \\ &\quad + U_{\text{sym},2}(\rho, k)(\tau\delta)^2 + \dots, \end{aligned} \quad (12)$$

where $U_0(\rho, k) \equiv U_n(\rho, 0, k) = U_p(\rho, 0, k)$ denotes the single-nucleon potential in symmetric nuclear matter and $U_{\text{sym},i}(\rho, k)$ denotes

$$\begin{aligned} U_{\text{sym},i}(\rho, k) &\equiv \frac{1}{i!} \frac{\partial^i U_n(\rho, \delta, k)}{\partial \delta^i} \Big|_{\delta=0} \\ &= \frac{(-1)^i}{i!} \frac{\partial^i U_p(\rho, \delta, k)}{\partial \delta^i} \Big|_{\delta=0}, \end{aligned} \quad (13)$$

with $U_{\text{sym},1}(\rho, k)$ being the well-known nuclear symmetry potential [8] (which is usually denoted by $U_{\text{sym}}(\rho, k)$) and $U_{\text{sym},2}(\rho, k)$ the second-order nuclear symmetry potential. Neglecting higher-order terms (i.e., $\delta^2, \delta^3, \dots$) in Eq. (12) leads to the well-known Lane approximation [53]

$$U_\tau(\rho, \delta, k) \approx U_0(\rho, k) + U_{\text{sym}}(\rho, k)(\tau\delta), \quad (14)$$

which has been extensively used to approximate the single-nucleon potential in asymmetric nuclear matter. Based on the Lane approximation, the symmetry potential $U_{\text{sym}}(\rho, k)$ can be evaluated approximately by [8, 54]

$$U_{\text{sym}}(\rho, k) \approx \frac{U_n(\rho, \delta, k) - U_p(\rho, \delta, k)}{2\delta}. \quad (15)$$

The nuclear symmetry potential is thus related to the isovector part of the nucleon mean-field potential in asymmetric nuclear matter. Besides the density, the nuclear symmetry potential also depends on the momentum or energy of a nucleon.

The nuclear symmetry potential is different from the nuclear symmetry energy since the latter involves the integration of the nucleon mean-field potential over the nucleon momentum. Therefore, the nuclear symmetry energy is a thermodynamic quantity while the nuclear symmetry potential is a dynamical quantity. On the other hand, based on the Hugenholtz-Van Hove theorem, it has been shown [55, 51, 52, 56] that both $E_{\text{sym}}(\rho)$ and $L(\rho)$ can be completely and analytically determined from the single-nucleon potential, especially the nuclear symmetry potential. Therefore, the nuclear symmetry energy and the nuclear symmetry potential are intrinsically correlated with each other. Experimentally, the single-nucleon potential (and thus the nuclear symmetry potential) can be obtained from the nucleon optical potential extracted from analyzing the nucleon-nucleus scattering data, (p,n) charge-exchange reactions between isobaric analog states, and single-particle energy levels of bound states. These data provide the possibility to extract information on the isospin dependence of the nucleon optical potential, especially the energy dependence of the nuclear symmetry potential [55, 57, 58].

3 Isospin- and momentum-dependent MDI interaction

In this Section, we review in detail the isospin- and momentum-dependent MDI interaction and its implementation in the Boltzmann-Uehling-Uhlenbeck (BUU) transport model. Also reviewed are some results on the properties of cold asymmetric nuclear matter obtained with the MDI interaction, such as the symmetry energy, the symmetry potential, the nucleon effective mass, and the in-medium NN elastic scattering cross sections.

3.1 The MDI interaction for transport model simulations

The nuclear single-particle potential (nuclear mean-field potential) is a basic input in the one-body transport models for heavy ion collisions, such as the BUU model (See, e.g., Ref. [59] for a review). It is through the nuclear mean-field potential that information on the nuclear matter EOS can be extracted from BUU-like transport model simulations for heavy ion collisions. In general, nuclear mean-field potentials are dependent on nucleon momentum [60, 61, 62, 63, 64, 65]. This is evident from the observed momentum/energy dependence of nucleon optical model potential, and can also be understood through the exchange-term contribution from the finite-range nuclear force. For transport model simulations for heavy ion collisions, Gale, Bertsch, and Das Gupta (GBD) [66] firstly introduced a parametrization of momentum-dependent mean-field potential in the BUU model. A more realistic parametrization of momentum-dependent mean-field potential, which correctly describes the extreme nonequilibrium situations in the early stage of heavy ion collisions, was later introduced in the BUU model by Welke *et al.* [67]. It is based on a finite-range nuclear force of the Yukawa form, and has thus been referred to as the momentum-dependent Yukawa interaction (MDYI) [67].

In original versions of both the GBD interaction and the MDYI interaction, the isospin dependence of nuclear mean-field potentials was neglected. However, the well-known Lane potential [53] as observed in the momentum/energy dependent nucleon optical model potential clearly demonstrated that the nuclear mean-field potentials should be isospin dependent. Such potentials are expected to be important for transport model simulations of heavy ion collisions induced by extremely neutron(proton)-rich nuclei. Bombaci [68] extended the GBD interaction to include explicitly the isospin dependence, resulting in the BGBD interaction. Similarly, the inclusion of isospin dependence in the more realistic MDYI interaction by Das *et al.* [69] leads to the so-called MDI interaction, which will be discussed in detail in the following.

The isospin- and momentum-dependent MDI interaction is a generalized isospin-dependent version of the MDYI interaction with its parameters obtained by fitting the single-particle potentials and nuclear matter EOS predicted by the finite-range Gogny effective interaction [69] using the parameter set D1 [61]. In the MDI interaction,

the potential energy density $V(\rho, \delta)$ of an asymmetric nuclear matter is parameterized as follows [69, 70]:

$$\begin{aligned}
 V(\rho, \delta) = & \frac{A_u(x)\rho_n\rho_p}{\rho_0} + \frac{A_l(x)}{2\rho_0}(\rho_n^2 + \rho_p^2) + \frac{B}{\sigma + 1} \frac{\rho^{\sigma+1}}{\rho_0^\sigma} \\
 & \times (1 - x\delta^2) + \frac{1}{\rho_0} \sum_{\tau, \tau'} C_{\tau, \tau'} \\
 & \times \int \int d^3p d^3p' \frac{f_\tau(\mathbf{r}, \mathbf{p}) f_{\tau'}(\mathbf{r}, \mathbf{p}')}{1 + (\mathbf{p} - \mathbf{p}')^2 / \Lambda^2}. \tag{16}
 \end{aligned}$$

In the mean-field approximation, Eq. (16) leads to the following single-nucleon potential [69, 70]:

$$\begin{aligned}
 U_\tau(\rho, \delta, \mathbf{p}) = & A_u(x) \frac{\rho_{-\tau}}{\rho_0} + A_l(x) \frac{\rho_\tau}{\rho_0} \\
 & + B \left(\frac{\rho}{\rho_0} \right)^\sigma (1 - x\delta^2) - 4\tau x \frac{B}{\sigma + 1} \frac{\rho^{\sigma-1}}{\rho_0^\sigma} \delta\rho_{-\tau} \\
 & + \frac{2C_l}{\rho_0} \int d^3p' \frac{f_\tau(\mathbf{r}, \mathbf{p}')}{1 + (\mathbf{p} - \mathbf{p}')^2 / \Lambda^2} \\
 & + \frac{2C_u}{\rho_0} \int d^3p' \frac{f_{-\tau}(\mathbf{r}, \mathbf{p}')}{1 + (\mathbf{p} - \mathbf{p}')^2 / \Lambda^2}. \tag{17}
 \end{aligned}$$

In the above, $f_\tau(\mathbf{r}, \mathbf{p})$ is the nucleon phase-space distribution function at coordinate \mathbf{r} and momentum \mathbf{p} . While the parameter $\sigma = 4/3$ follows that from the Gogny interaction, the other six parameters $A_u(x)$, $A_l(x)$, B , $C_{\tau, \tau}$ ($\equiv C_l$), $C_{\tau, -\tau}$ ($\equiv C_u$), and Λ are obtained by fitting the momentum dependence of single-nucleon potential to that predicted by the Gogny Hartree-Fock (and/or the Brueckner-Hartree-Fock) calculations, the saturation properties of symmetric nuclear matter, and the symmetry energy of 30.5 MeV at nuclear matter saturation density $\rho_0 = 0.16 \text{ fm}^{-3}$ [69]. The incompressibility K_0 of cold symmetric nuclear matter at ρ_0 is set to be 211 MeV.

The parameters $A_u(x)$ and $A_l(x)$ depend on the parameter x according to

$$A_u(x) = A_{u0} - x \frac{2B}{\sigma + 1}, \quad A_l(x) = A_{l0} + x \frac{2B}{\sigma + 1}, \tag{18}$$

with $A_{u0} = A_u(x = 0) = -95.98 \text{ MeV}$ and $A_{l0} = A_l(x = 0) = -120.57 \text{ MeV}$. Varying the value of x allows one to obtain different density dependence of the nuclear symmetry energy while keeping the value of $E_{\text{sym}}(\rho_0) = 30.5 \text{ MeV}$ and other properties of symmetric nuclear matter unchanged [70]. It thus can be adjusted to mimic the predictions of microscopic and/or phenomenological many-body theories on the density dependence of nuclear matter symmetry energy. The x parameter can be related to the well-known x_3 parameter in the density-dependent part of the Skyrme (and Gogny) interaction [71], i.e.,

$$v_3(\mathbf{r}_1, \mathbf{r}_2) = \frac{1}{6} t_3 (1 + x_3 P_\sigma) \left[\rho \left(\frac{\mathbf{r}_1 + \mathbf{r}_2}{2} \right) \right]^\gamma \delta(\mathbf{r}_1 - \mathbf{r}_2), \tag{19}$$

by

$$x = (1 + 2x_3)/3. \tag{20}$$

In Eq. (19), γ is the density-dependence parameter used to mimic in-medium effects of the many-body interactions ($\gamma = \sigma - 1$), and with $\gamma = 1$ it represents an effective density-dependent two-body interaction deduced from a three-body contact interaction in spin-saturated nuclear matter [27]. The x_3 is the spin (isospin)-dependence parameter controlling the relative contributions of the density-dependent term to the total energy in the isospin singlet ($T = 0$) channel ($\propto (1 + x_3)\rho^{\gamma+1}$) and triplet ($T = 1$) channel ($\propto (1 - x_3)\rho^{\gamma+1}$) (see, e.g., Ref. [61] for details). In particular, we note that $x_3 = 1$ ($x_3 = -1$) means the density-dependent term only contributes to the $T = 0$ ($T = 1$) channel. Therefore, varying x from 1 to -1 in the MDI interaction can cover a large range of uncertainties due to the spin (isospin)-dependence of the in-medium many-body interactions. As a matter of fact, one main reason for the rather divergent density dependence of the nuclear symmetry energy in various Skyrme and/or Gogny Hartree-Fock calculations [72] is due to the different values of x_3 or x parameter [73]. On the other hand, it should be pointed out that the parameter x or x_3 does not affect the EOS of symmetric nuclear matter since its contributions from $T = 0$ and $T = 1$ channels are exactly canceled, i.e., $\propto (1 + x_3)\rho^{\gamma+1} + (1 - x_3)\rho^{\gamma+1} = 2\rho^{\gamma+1}$. Also, by the construction in Eq. (18), the x or x_3 parameter does not change the symmetry energy value at ρ_0 from the MDI interaction either. As to the parameter B , it is related to the t_3 term in the Skyrme (and Gogny) effective interaction via $B = t_3(\sigma + 1)\rho_0^\sigma/16$, and particularly we have $B = 106.35$ MeV in the MDI interaction.

The last two terms in Eq. (17) represent the momentum dependence of the single-nucleon potential. The momentum dependence of the symmetry potential comes from the different interaction strength parameters C_l and C_u for a nucleon of isospin τ interacting, respectively, with like and unlike nucleons in the nuclear matter. In particular, we have $C_l = -11.7$ MeV and $C_u = -103.4$ MeV in the MDI interaction.

As shown in Ref. [74], an explicit form for an NN interaction, which leads to a potential energy density similar to that given in Eq. (16) for the MDI interaction, can be obtained by assuming that the interaction potential between two nucleons located at \mathbf{r}_1 and \mathbf{r}_2 has the following form:

$$v(\mathbf{r}_1, \mathbf{r}_2) = \frac{1}{6}t_3(1 + x_3P_\sigma)\rho^\gamma \left(\frac{\mathbf{r}_1 + \mathbf{r}_2}{2} \right) \delta(\mathbf{r}_1 - \mathbf{r}_2) + (W + GP_\sigma - HP_\tau - MP_\sigma P_\tau) \frac{e^{-\mu|\mathbf{r}_1 - \mathbf{r}_2|}}{|\mathbf{r}_1 - \mathbf{r}_2|}. \quad (21)$$

The above interaction has the same form as the Gogny interaction [61,69] except that the two finite-range Gaussian terms in the Gogny interaction are replaced by a single Yukawa form. We would like to point out that a more general finite-range effective NN interaction, which has all the four spin-parity components, i.e., singlet-even (SE), triplet-even (TE), singlet-odd (SO) and triplet-odd (TO) as well as more general forms for the finite-range terms

such as Yukawa, Gaussian and exponential, has been proposed in Ref. [65] and applied to study the momentum and density dependence of the nuclear mean-field potential in symmetric nuclear matter as well as the corresponding EOS. The same formalism has been subsequently applied to systematically investigate neutron and proton mean-field potentials, the thermodynamic properties of highly isospin asymmetric nuclear matter, and the properties of neutron stars [75,76,77,78]. The eight parameters (including x_3) in the above NN interaction (i.e., Eq. (21)) can be uniquely related to the eight parameters (including x) in the MDI interaction (see the energy density functional of Eq. (16)) through the following relations:

$$t_3 = \frac{16B}{(\sigma + 1)\rho_0^\sigma}, \quad (22)$$

$$x_3 = \frac{3x - 1}{2}, \quad (23)$$

$$\gamma = \sigma - 1, \quad (24)$$

$$\mu = \Lambda, \quad (25)$$

$$W = \frac{\Lambda^2}{3\pi\rho_0}(A_1 - A_2 + C_l - C_u), \quad (26)$$

$$G = \frac{\Lambda^2}{6\pi\rho_0}(-A_1 + A_2 - 4C_l + 4C_u), \quad (27)$$

$$H = \frac{\Lambda^2}{3\pi\rho_0}(-2A_2 - C_u), \quad (28)$$

$$M = \frac{\Lambda^2}{3\pi\rho_0}(A_2 + 2C_u), \quad (29)$$

with $A_1 = [A_l(x) + A_u(x)]/2$ and $A_2 = [A_l(x) - A_u(x)]/2$.

It should be mentioned that the MDI interaction has been extensively applied in the transport model simulations for studying isospin effects in intermediate-energy heavy ion collisions induced by neutron-rich nuclei [70, 79,80,81,82,83,84,85,86,87] as well as the study on the thermal properties of asymmetric nuclear matter [88,89,90] and the properties of neutron stars [47,48]. We will highlight some results in the following.

3.2 Cold asymmetric nuclear matter with the MDI interaction

Although the nucleon phase space distribution function $f_\tau(\mathbf{r}, \mathbf{p})$ in Eq. (16) and Eq. (17) is for nuclear matter not necessary in equilibrium, it is instructive to examine the equilibrium case. For cold nuclear matter at zero temperature, one has $f_\tau(\mathbf{r}, \mathbf{p}) = \frac{2}{h^3}\Theta(p_{F,\tau} - p)$ with $p_{F,\tau} = \hbar(3\pi^2\rho_\tau)^{1/3}$ being the Fermi momentum of nucleons of isospin τ in asymmetric nuclear matter, and the integrals in Eqs. (16) and (17) can be analytically evaluated [69,

91], leading to

$$\begin{aligned}
& \int \int d^3\mathbf{p} d^3\mathbf{p}' \frac{f_\tau(\mathbf{r}, \mathbf{p}) f_{\tau'}(\mathbf{r}, \mathbf{p}')}{1 + (\mathbf{p} - \mathbf{p}')^2 / \Lambda^2} \\
&= \frac{1}{6} \left(\frac{4\pi}{h^3} \right)^2 \Lambda^2 \left\{ p_{F,\tau} p_{F,\tau'} [3(p_{F,\tau}^2 + p_{F,\tau'}^2) - \Lambda^2] \right. \\
&+ 4\Lambda [(p_{F,\tau}^3 - p_{F,\tau'}^3) \arctan \frac{p_{F,\tau} - p_{F,\tau'}}{\Lambda} \\
&- (p_{F,\tau}^3 + p_{F,\tau'}^3) \arctan \frac{p_{F,\tau} + p_{F,\tau'}}{\Lambda}] \\
&+ \frac{1}{4} [\Lambda^4 + 6\Lambda^2(p_{F,\tau}^2 + p_{F,\tau'}^2) - 3(p_{F,\tau}^2 - p_{F,\tau'}^2)^2] \\
&\times \ln \frac{(p_{F,\tau} + p_{F,\tau'})^2 + \Lambda^2}{(p_{F,\tau} - p_{F,\tau'})^2 + \Lambda^2} \left. \right\} \quad (30)
\end{aligned}$$

and

$$\begin{aligned}
& \int d^3\mathbf{p}' \frac{f_\tau(\mathbf{r}, \mathbf{p}')}{1 + (\mathbf{p} - \mathbf{p}')^2 / \Lambda^2} \\
&= \frac{2}{h^3} \pi \Lambda^3 \left[\frac{p_{F,\tau}^2 + \Lambda^2 - p^2}{2p\Lambda} \ln \frac{(p + p_{F,\tau})^2 + \Lambda^2}{(p - p_{F,\tau})^2 + \Lambda^2} \right. \\
&+ \left. \frac{2p_{F,\tau}}{\Lambda} - 2(\arctan \frac{p + p_{F,\tau}}{\Lambda} - \arctan \frac{p - p_{F,\tau}}{\Lambda}) \right]. \quad (31)
\end{aligned}$$

The kinetic energy contribution to the binding energy per nucleon in cold asymmetric nuclear matter can be obtained as

$$\begin{aligned}
E_K(\rho, \delta) &= \frac{1}{\rho} \int d^3\mathbf{p} \left[\frac{p^2}{2m} f_n(\mathbf{r}, \mathbf{p}) + \frac{p^2}{2m} f_p(\mathbf{r}, \mathbf{p}) \right] \\
&= \frac{4\pi}{5mh^3\rho} (p_{F,n}^5 + p_{F,p}^5), \quad (32)
\end{aligned}$$

and the total binding energy per nucleon of cold asymmetric nuclear matter then can be expressed as

$$E(\rho, \delta) = E_K(\rho, \delta) + \frac{V(\rho, \delta)}{\rho}. \quad (33)$$

By setting $\rho_n = \rho_p = \rho/2$ and $p_{F,n} = p_{F,p} = p_F$, one obtains the following EOS of cold symmetric nuclear matter:

$$\begin{aligned}
E_0(\rho) &= \frac{8\pi}{5mh^3\rho} p_F^5 + \frac{\rho}{4\rho_0} [A_l(x) + A_u(x)] \\
&+ \frac{B}{\sigma + 1} \left(\frac{\rho}{\rho_0} \right)^\sigma + \frac{1}{3\rho_0\rho} (C_l + C_u) \left(\frac{4\pi}{h^3} \right)^2 \Lambda^2 \\
&\times \left[p_F^2 (6p_F^2 - \Lambda^2) - 8\Lambda p_F^3 \arctan \frac{2p_F}{\Lambda} \right. \\
&+ \left. \frac{1}{4} (\Lambda^4 + 12\Lambda^2 p_F^2) \ln \frac{4p_F^2 + \Lambda^2}{\Lambda^2} \right]. \quad (34)
\end{aligned}$$

It should be mentioned that, as expected, the $E_0(\rho)$ is independent of the parameter x since $A_l(x) + A_u(x) = A_{l0} + A_{u0} = -216.55$ MeV is a constant according to Eq. (18).

By definition, the symmetry energy can be obtained as

$$\begin{aligned}
E_{\text{sym}}(\rho) &= \frac{1}{2} \left(\frac{\partial^2 E}{\partial \delta^2} \right)_{\delta=0} \\
&= \frac{8\pi}{9mh^3\rho} p_f^5 + \frac{\rho}{4\rho_0} (A_l(x) - A_u(x)) - \frac{Bx}{\sigma + 1} \left(\frac{\rho}{\rho_0} \right)^\sigma \\
&+ \frac{C_l}{9\rho_0\rho} \left(\frac{4\pi}{h^3} \right)^2 \Lambda^2 \left[4p_F^4 - \Lambda^2 p_F^2 \ln \frac{4p_F^2 + \Lambda^2}{\Lambda^2} \right] \\
&+ \frac{C_u}{9\rho_0\rho} \left(\frac{4\pi}{h^3} \right)^2 \Lambda^2 \left[4p_F^4 - p_F^2 (4p_F^2 + \Lambda^2) \ln \frac{4p_F^2 + \Lambda^2}{\Lambda^2} \right]. \quad (35)
\end{aligned}$$

Since $A_l(x) - A_u(x) = A_{l0} - A_{u0} + 4Bx/(\sigma + 1)$ according to Eq. (18), the $E_{\text{sym}}(\rho)$ depends linearly on the parameter x at a given density except ρ_0 where the symmetry energy is independent of x and its value is fixed by construction. As an example, we show in Fig. 1 the density dependence of the symmetry energy in the MDI interaction with $x = 1, 0, -1, \text{ and } -2$. As expected, one can see that varying the value of x in the MDI interaction leads to a very broad range of the density dependence of the nuclear symmetry energy, similar to those predicted by various microscopic and phenomenological many-body approaches.

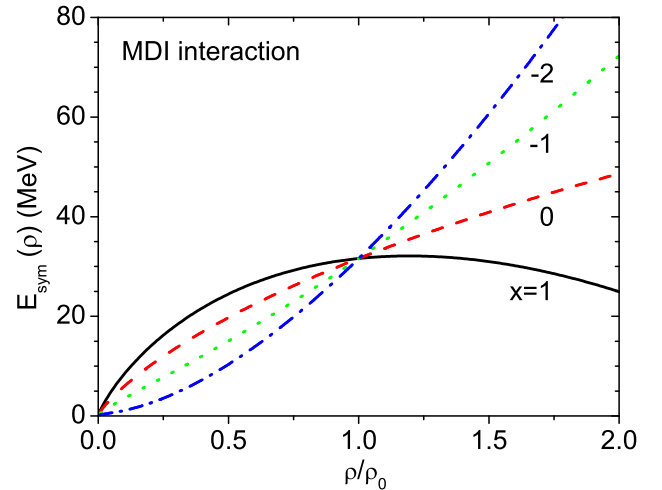


Fig. 1. (Color online) Symmetry energy as a function of density for the MDI interaction with $x = 1, 0, -1, \text{ and } -2$. Taken from Ref. [70].

The single-nucleon potential for a nucleon of momentum p and isospin τ in cold asymmetric nuclear matter

can be expressed as

$$\begin{aligned}
U_\tau(\rho, \delta, p) = & A_u(x) \frac{\rho_{-\tau}}{\rho_0} + A_l(x) \frac{\rho_\tau}{\rho_0} \\
& + B \left(\frac{\rho}{\rho_0} \right)^\sigma (1 - x\delta^2) - 4\tau x \frac{B}{\sigma + 1} \frac{\rho^{\sigma-1}}{\rho_0^\sigma} \delta \rho_{-\tau} \\
& + \frac{2C_l}{\rho_0} \frac{2}{\hbar^3} \pi \Lambda^3 \left[\frac{p_{F,\tau}^2 + \Lambda^2 - p^2}{2p\Lambda} \ln \frac{(p + p_{F,\tau})^2 + \Lambda^2}{(p - p_{F,\tau})^2 + \Lambda^2} \right. \\
& \left. + \frac{2p_{F,\tau}}{\Lambda} - 2 \arctan \frac{p + p_{F,\tau}}{\Lambda} + 2 \arctan \frac{p - p_{F,\tau}}{\Lambda} \right] \\
& + \frac{2C_u}{\rho_0} \frac{2}{\hbar^3} \pi \Lambda^3 \left[\frac{p_{F,-\tau}^2 + \Lambda^2 - p^2}{2p\Lambda} \ln \frac{(p + p_{F,-\tau})^2 + \Lambda^2}{(p - p_{F,-\tau})^2 + \Lambda^2} \right. \\
& \left. + \frac{2p_{F,-\tau}}{\Lambda} - 2 \arctan \frac{p + p_{F,-\tau}}{\Lambda} + 2 \arctan \frac{p - p_{F,-\tau}}{\Lambda} \right]. \quad (36)
\end{aligned}$$

In cold symmetric nuclear matter with $\rho_n = \rho_p = \rho/2$, the single-nucleon potential thus is

$$\begin{aligned}
U_0(\rho, p) = & \frac{A_l(x) + A_u(x)}{2} \frac{\rho}{\rho_0} + B \left(\frac{\rho}{\rho_0} \right)^\sigma \\
& + \frac{2(C_{\tau,\tau} + C_{\tau,-\tau})}{\rho_0} \frac{2}{\hbar^3} \pi \Lambda^3 \left[\frac{p_F^2 + \Lambda^2 - p^2}{2p\Lambda} \ln \frac{(p + p_F)^2 + \Lambda^2}{(p - p_F)^2 + \Lambda^2} \right. \\
& \left. + \frac{2p_F}{\Lambda} - 2 \arctan \frac{p + p_F}{\Lambda} + 2 \arctan \frac{p - p_F}{\Lambda} \right], \quad (37)
\end{aligned}$$

and the nuclear symmetry potential by definition (i.e., Eq. (13)) is

$$\begin{aligned}
U_{\text{sym},1}(\rho, p) = & \frac{A_l(x) - A_u(x)}{2} \frac{\rho}{\rho_0} - 2x \frac{B}{\sigma + 1} \left(\frac{\rho}{\rho_0} \right)^\sigma \\
& + \frac{2(C_{\tau,\tau} - C_{\tau,-\tau})}{\rho_0} \frac{2\pi p_F^2 \Lambda^2}{3\hbar^3 p} \ln \frac{(p + p_F)^2 + \Lambda^2}{(p - p_F)^2 + \Lambda^2}. \quad (38)
\end{aligned}$$

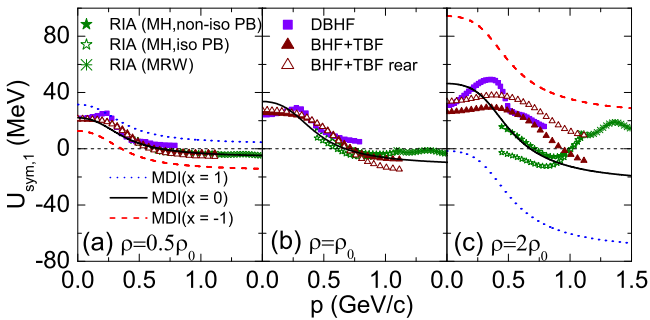


Fig. 2. (Color online) Momentum dependence of the symmetry potential $U_{\text{sym},1}(\rho, k)$ at $\rho = 0.5\rho_0$ (a), ρ_0 (b), and $2\rho_0$ (c) using the MDI interaction with $x = -1, 0$, and 1 . Corresponding results from several microscopic approaches are also included for comparison (See the text for details). Taken from Ref. [52].

Shown in Fig. 2 is the momentum dependence of $U_{\text{sym},1}(\rho, k)$ (i.e., $U_{\text{sym}}(\rho, k)$) at $\rho = 0.5\rho_0$, ρ_0 , and $2\rho_0$ in the MDI interaction with $x = -1, 0$, and 1 . For comparison, we also

include in Fig. 2 corresponding results from several microscopic approaches, including the non-relativistic Brueckner-Hartree-Fock (BHF) theory with and without the rearrangement contribution from the three-body force (TBF) [92], the relativistic Dirac-Brueckner-Hartree-Fock (DBHF) theory [93], and the relativistic impulse approximation (RIA) [94, 95] using the empirical NN scattering amplitude determined by Murdock and Horowitz (MH) [96] as well as by McNeil, Ray, and Wallace (MRW) [97] with isospin-dependent and isospin-independent Pauli blocking corrections. It is seen that these microscopic results are essentially consistent with each other around and below ρ_0 although large uncertainties still exist at higher density $\rho = 2\rho_0$. It is interesting to note that the $U_{\text{sym}}(\rho, k)$ from the MDI interaction with $x = 0$, which decreases with the nucleon momentum, is in good agreement with the results from the microscopic approaches at all densities shown in Fig. 2.

3.3 Nucleon effective mass and in-medium nucleon-nucleon scattering cross section with the MDI interaction

The nucleon effective mass is an important physical quantity that reflects the momentum dependence of the nuclear mean-field potential in nuclear matter. In isospin asymmetric nuclear matter, the nucleon effective mass m_τ^* is given by

$$\frac{m_\tau^*}{m_\tau} = \left\{ 1 + \frac{m_\tau}{p} \frac{dU_\tau}{dp} \right\}^{-1}, \quad (39)$$

and it can be different for protons and neutrons. It normally depends on the density and isospin asymmetry of the medium as well as the momentum of the nucleon [98, 99, 100]. The well-known Landau mass which is related to the Landau parameter f_1 of a Fermi liquid [98, 99, 100] corresponds to the nucleon effective mass evaluated at the Fermi momentum $p_\tau = p_{F,\tau}$ in Eq. (39). A detailed discussion about different kinds of effective masses can be found in Refs. [98, 91]. It should be mentioned that the nucleon effective masses from the MDI interaction are independent of the x parameter because the momentum-dependent part of the single-nucleon potential in Eq. (17) is independent of the parameter x .

Figure 3 displays the results from the MDI interaction for the effective masses of neutrons and protons in cold asymmetric nuclear matter at their respective Fermi surfaces (i.e., Landau mass) as functions of density (upper window) and isospin asymmetry (lower window). One can see that the neutron has a larger effective mass than the proton in neutron-rich matter and the effective mass splitting between them increases with both the density and isospin asymmetry of the nuclear medium. It should be noted that the neutron-proton effective mass splitting is related to the momentum dependence of the symmetry potential [54, 55]. The larger neutron effective mass than proton effective mass in neutron-rich matter essentially reflects the fact that the symmetry potential decreases with nucleon momentum as shown in Fig. 2, which is consistent

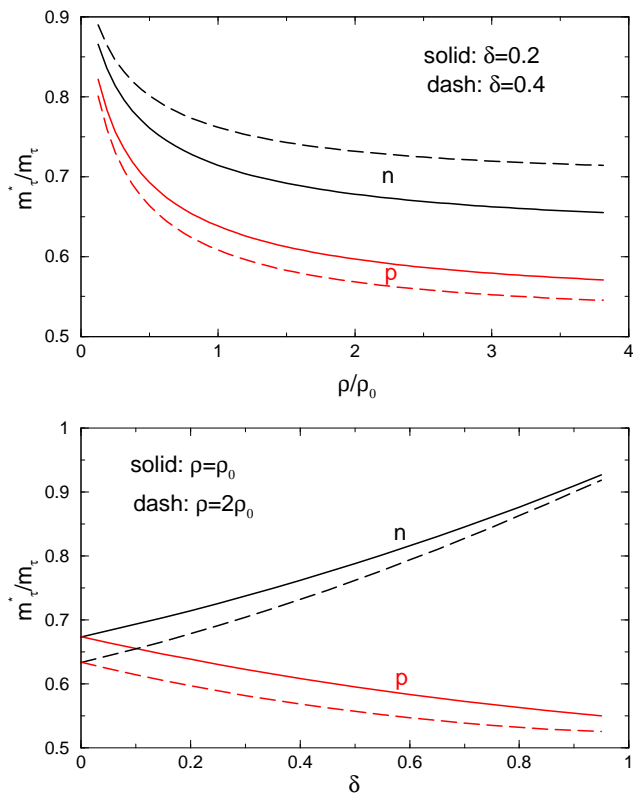


Fig. 3. (Color online) Neutron and proton effective masses in asymmetric nuclear matter as functions of density (upper window) and isospin asymmetry (lower window) from the MDI interaction. Taken from Ref. [83].

with calculations from many phenomenological and microscopic models, see, e.g., Refs. [12, 100, 101, 102, 103, 104] as well as the symmetry potential extracted from empirical isospin-dependent optical model potentials [55, 57, 105].

Besides the mean-field potential, another basic component in transport models is the NN scattering cross sections. In principle, both nuclear mean-field potentials and NN scattering cross sections should be determined self-consistently from the same interaction. In practice, however, due to the complexity of the problem, the nuclear mean-field potentials and NN scattering cross sections are usually modeled separately in transport model simulations of heavy ion collisions. Especially, the experimental free space NN scattering cross sections (or with simple constant or local density-dependent scalings) are usually used in many transport model simulations. In the IBUU04 transport model, the option of using in-medium NN cross sections is included by extending the effective mass scaling model [106, 107, 108] to isospin asymmetric matter using the isospin- and momentum-dependent MDI interaction. In the effective mass scaling model, the NN interaction matrix elements in the medium are assumed to be the same as that in free-space. The NN cross sections in the medium ($\sigma_{NN}^{\text{medium}}$) thus differ from those in free space ($\sigma_{NN}^{\text{free}}$) only due to the difference in the incoming current in the initial state and the density of states in

the final state. Since both depend on the effective masses of a colliding nucleon pair, the NN cross sections are thus reduced in the medium by the factor

$$R_{\text{medium}} \equiv \sigma_{NN}^{\text{medium}} / \sigma_{NN}^{\text{free}} = (\mu_{NN}^* / \mu_{NN})^2, \quad (40)$$

where μ_{NN} and μ_{NN}^* are, respectively, the reduced masses of the colliding nucleon pair in free-space and in the medium.

It should be pointed out that the scaling of $\sigma_{NN}^{\text{medium}} / \sigma_{NN}^{\text{free}}$ in Eq. (40) is consistent with calculations based on the DBHF theory [109] for colliding nucleon pairs with relative momenta less than about 240 MeV/c at densities less than about $2\rho_0$. This provides a strong support for the effective mass scaling model in the limited density and momentum ranges, and the scaling model to elastic NN scatterings can thus be safely applied in the transport model simulations for heavy-ion collisions at beam energies up to about the pion production threshold. For heavy-ion collisions at higher energies, inelastic reaction channels become important and in-medium effects on these channels have been a subject of much interest [110, 111, 112]. In the IBUU04 model, the experimental free-space cross sections are, however, used for the inelastic channels.

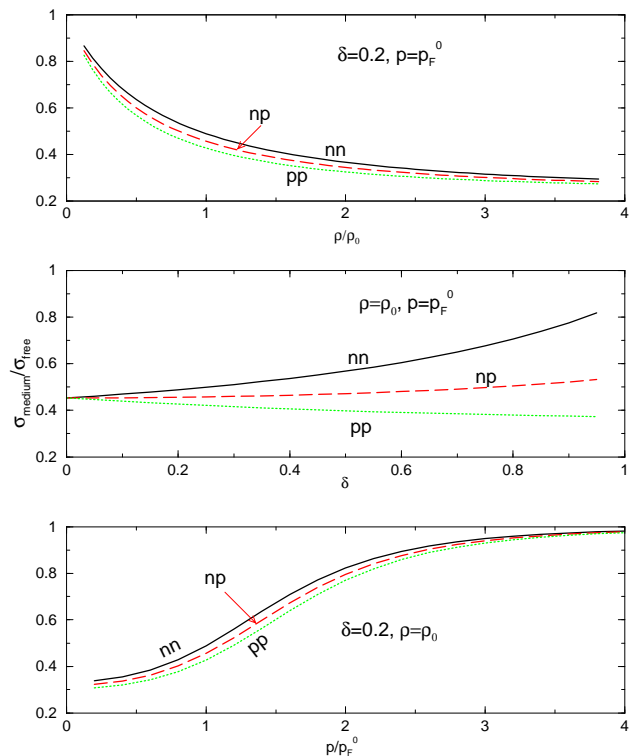


Fig. 4. (Color online) Ratio of NN cross sections in nuclear medium to their free-space values as a function of density (top window), isospin asymmetry (middle window), and momentum (bottom window). Taken from Ref. [83].

In transport model simulations of heavy-ion collisions, the nucleon effective masses used to obtain the in-medium NN cross sections within the effective mass scaling model have to be evaluated dynamically in the evolving medium

created during the collisions [83]. As an example of a simplified case, it is instructive to see the in-medium NN cross sections in cold asymmetric nuclear matter in equilibrium. In this case, the nucleon effective mass can be obtained analytically and analytical expressions of the medium reduction factor R_{medium} can thus also be obtained, albeit lengthy. Shown in Fig. 4 is the reduction factor R_{medium} for two colliding nucleons having the same magnitude of momentum p as a function of density (upper window), isospin asymmetry (middle window), and the nucleon momentum (bottom window). It is interesting to see that not only the in-medium NN cross sections are reduced compared with their free-space values, but the nn cross sections are larger than the pp cross sections in the neutron-rich matter although their free-space values are the same. Moreover, the difference between the nn and pp scattering cross sections becomes larger in more neutron-rich matter. The larger in-medium cross sections for nn scatterings than for pp scatterings in neutron-rich matter are completely due to the positive n-p effective mass splitting in neutron-rich matter with the MDI interaction as shown in Fig. 3. This feature provides a potential probe of the n-p effective mass splitting in neutron-rich matter and can be studied in heavy ion collisions induced by neutron-rich nuclei. It should be noted that the in-medium NN cross sections are also independent of the x parameter in the MDI interaction and they are solely determined by the nucleon effective masses through the momentum dependence of the single-nucleon potential used in the effective mass scaling model.

4 Applications of the isospin- and momentum-dependent MDI interaction

In this Section, we highlight some applications of the MDI interaction in studying heavy ion collisions based on transport model simulations, the thermal properties of asymmetric nuclear matter, and the properties of neutron stars. These studies have allowed us to extract many useful information about the isospin and momentum dependence of the in-medium nuclear effective interaction.

4.1 Heavy ion collisions

The first application of the MDI interaction was done by Li *et al.* [79] in BUU transport model simulations of heavy ion collisions induced by neutron-rich nuclei at intermediate energies. They found that the symmetry potentials with and without the momentum dependence but corresponding to the same density-dependent symmetry energy would lead to significantly different predictions on several symmetry energy sensitive experimental observables. The momentum dependence of the symmetry potential is thus very important for exploring accurately the EOS and properties of dense neutron-rich matter. Since then, the BUU transport model with the MDI interaction has been extensively used for investigating the isospin effects

in heavy ion collisions and for extracting information on the density dependence of the symmetry energy (See, e.g., Ref. [8]). The BUU transport model with the MDI interaction has also been applied to constrain the high-density behaviors of the symmetry energy by analyzing the FOPI data on charged pion ratio in heavy ion collisions [113, 114, 115] as well as photon production in those collisions [116] (See, also Ref. [117]). In this subsection, we only highlight two of these extensive studies, i.e., the isospin diffusion/transport and $t/{}^3\text{He}$ ratio, with emphasis on the importance of the momentum dependence of the mean-field potential, especially the momentum dependence of the symmetry potential in heavy ion collisions induced by neutron-rich nuclei.

4.1.1 Isospin diffusion/transport

One important application [70] of the MDI interaction is the analysis of the isospin diffusion (transport) data from NSCL-MSU [118] within the IBUU04 transport model. Experimentally, the degree of isospin diffusion between the projectile nucleus A and the target nucleus B can be studied via the physical quantity R_i [119, 118] defined as

$$R_i = \frac{2X^{A+B} - X^{A+A} - X^{B+B}}{X^{A+A} - X^{B+B}}, \quad (41)$$

where X is an isospin-sensitive observable. One can see that the value of R_i is 1 (-1) for symmetric $A+A$ ($B+B$) reaction by construction. If isospin equilibrium is reached during the collision due to isospin diffusion, the value of R_i becomes about zero. In the NSCL/MSU experiments with $A = {}^{124}\text{Sn}$ and $B = {}^{112}\text{Sn}$ at a beam energy of 50 MeV/nucleon and an impact parameter about 6 fm, the isospin asymmetry of the projectile-like residue was used as the isospin tracer X [118].

Shown in Fig. 5 is the degree of the isospin diffusion $1 - R_i$ as a function of the slope L of the symmetry energy at saturation density obtained from the IBUU04 transport model with different mean-field potentials and NN cross sections, i.e., the MDI interaction with in-medium NN cross sections that are consistent with the mean-field potential obtained with the MDI interactions via the effective mass scaling model (MDI + σ_{med}), the MDI interaction with free-space experimental NN cross sections (MDI + σ_{exp}), and the momentum-independent soft Bertsch-Kruse-Das Gupta (SBKD) [120] mean-field potential with free-space experimental NN cross sections. For the momentum-independent SBKD mean-field potential, the momentum-independent symmetry potential obtained from the same density-dependent symmetry energy with different x values has been used [70]. The shaded band in Fig. 5 indicates the data from NSCL/MSU [118]. It is seen from Fig. 5 that for the SBKD interaction without momentum dependence, the isospin diffusion decreases monotonically (i.e., increasing value for R_i) with increasing L . The isospin diffusion is reduced when the isospin- and momentum-dependent MDI interaction (with σ_{exp}) is used because the momentum dependence weakens the strength of symmetry potential except for $x = -2$. As seen in Fig. 3

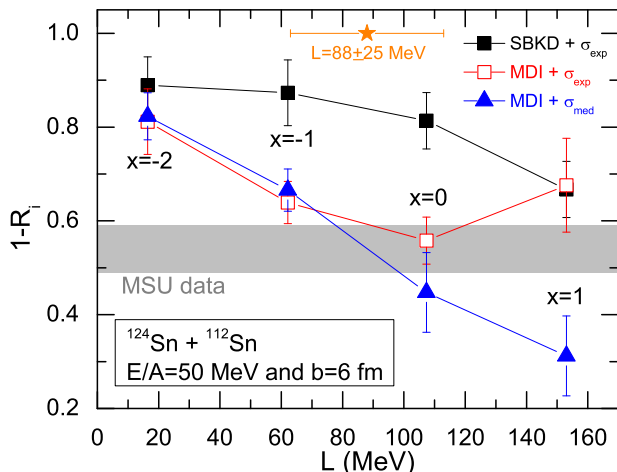


Fig. 5. (Color online) Degree of the isospin diffusion $1 - R_i$ as a function of L using the SBKD interaction with the free-space experimental nucleon-nucleon cross sections σ_{exp} (SBKD + σ_{exp}), the MDI interaction with σ_{exp} (MDI + σ_{exp}), and the MDI interaction with the in-medium nucleon-nucleon cross sections (MDI + σ_{med}). The $x = -2, -1, 0,$ and 1 indicate the different symmetry energies in the MDI interaction and the shaded band indicates the data from NSCL/MSU [118]. The solid star with error bar represents $L = 88 \pm 25$ MeV. The calculated results are taken from Refs. [70, 83].

of Ref. [70], the symmetry potential in the MDI interaction has the smallest strength for $x = -1$ as it is close to zero at $k \approx 1.5 \text{ fm}^{-1}$ and $\rho/\rho_0 \approx 0.5$, and increases again with further stiffening of the symmetry energy, e.g., $x = -2$, when it becomes largely negative at all momenta and densities. The MDI interaction with $x = -1$ thus gives the smallest degree of isospin diffusion among the interactions considered and reproduces the MSU data. If the isoscalar part of the SBKD potential is replaced with the momentum-dependent (but isospin-independent) MDYI potential, which has a similar K_0 as those for the MDI and SBKD interactions, the resulting $R_i = 0.37 \pm 0.07$ is close to that obtained in the MDI interaction ($R_i = 0.44 \pm 0.05$) with $x = -1$, implying that the momentum dependence of the symmetry potential introduced in the MDI interaction leads to about 16% variation for the isospin diffusion.

Furthermore, one can see from Fig. 5 that the difference in $1 - R_i$ obtained with the free-space (MDI + σ_{exp}) and the in-medium (MDI + σ_{med}) NN cross sections using the same MDI interaction is about the same for $x = -2$ and $x = -1$, but becomes especially large at $x = 0$ and $x = 1$. As pointed out in Ref. [83], these results can be understood by considering contributions from the symmetry potential and the np scatterings. Schematically, the mean-field contribution is proportional to the product of the isospin asymmetric force F_{np} and the inverse of the np scattering cross section σ_{np} [121]. While the collisional contribution is proportional to σ_{np} , the overall effect of NN cross sections on isospin diffusion is a result of a complicated combination of the effects due to both the nuclear mean field and NN scatterings. Generally speaking, while the symmetry potential effects on the isospin diffusion be-

come weaker when the NN cross sections are larger, the symmetry potential effects would show up more clearly if NN cross sections are smaller.

From comparison of the theoretical results with MDI + σ_{med} to the data, one can extract a value of $L = 88 \pm 25$ MeV, shown by the solid star with error bar in Fig. 5. This value (and $E_{\text{sym}}(\rho_0) = 31.6$ MeV) has been obtained with the parabolic approximation (i.e., Eq (3)) for the symmetry energy. Without using the parabolic approximation, the constraint changes slightly to $L = 86 \pm 25$ MeV with $E_{\text{sym}}(\rho_0) = 30.5$ MeV. This nuclear symmetry energy is significantly softer than the prediction by transport model simulation with a momentum-independent interaction [118] but is in agreement with a number of microscopic theoretical calculations. These results indicate that the isospin diffusion in heavy ion collisions indeed provides a sensitive probe of the isospin- and momentum-dependent nuclear effective interaction and corresponding in-medium NN scattering cross sections.

4.1.2 $t/{}^3\text{He}$ ratio

While the neutron/proton ratios of preequilibrium nucleons [122] and squeezed-out nucleons [87] in heavy ion collisions induced by neutron-rich nuclei have been shown to be sensitive probes of the density dependence of the symmetry energy, they suffer from some practical difficulties since it is hard to measure neutrons accurately in experiments. On the other hand, for light charged clusters such as deuteron (d), triton (t), and ${}^3\text{He}$, their yields and ratios have also been shown to be sensitive to the density dependence of the symmetry energy [123, 80], and compared to neutrons they can be measured much easier in experiments.

Light cluster production has been extensively investigated in experiments involving heavy ion collisions at all energies (see, e.g., Ref. [124] for a review). A popular model for describing the production of light clusters in these collisions is the coalescence model, e.g., see Ref. [125] for a theoretical review, which has been used at both intermediate [126, 127, 128, 129] and high energies [130, 131]. In this model, the cluster production probability is determined by the overlap of its Wigner phase-space density with the phase-space distribution of nucleons at freeze out in a heavy ion collision. Explicitly, the multiplicity of an M -nucleon cluster is given by [130]

$$N_M = G \int d\mathbf{r}_{i_1} d\mathbf{q}_{i_1} \cdots d\mathbf{r}_{i_{M-1}} d\mathbf{q}_{i_{M-1}} \langle \sum_{i_1 > i_2 > \cdots > i_M} \rho_i^W(\mathbf{r}_{i_1}, \mathbf{q}_{i_1} \cdots \mathbf{r}_{i_{M-1}}, \mathbf{q}_{i_{M-1}}) \rangle. \quad (42)$$

In the above, G is the spin-isospin statistical factor for the cluster [132]; $\mathbf{r}_{i_1}, \cdots, \mathbf{r}_{i_{M-1}}$ and $\mathbf{q}_{i_1}, \cdots, \mathbf{q}_{i_{M-1}}$ are, respectively, the $M - 1$ relative coordinates and momenta taken at equal time in the rest frame of the M nucleons; ρ_i^W is the Wigner phase-space density of the M -nucleon cluster; and $\langle \cdots \rangle$ means event averaging. Details about such calculation can be found in Ref. [123].

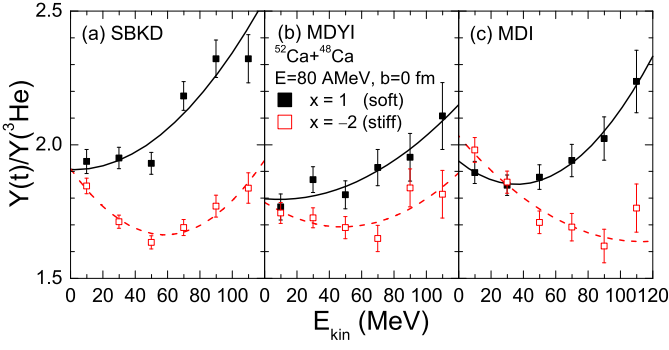


Fig. 6. (Color online) The cluster kinetic energy dependence of the $t/{}^3\text{He}$ ratio for interactions SBKD (a), MDYI (b), and MDI (c) with the soft (solid squares) and stiff (open squares) symmetry energies. The lines are drawn to guide eyes. Taken from Ref. [80].

The isobaric yield ratio $t/{}^3\text{He}$ is less dependent on the isoscalar properties of the nuclear mean-field potential and also less affected by other effects, such as the feedback from heavy fragment evaporation and from excited triton and ${}^3\text{He}$ states produced in heavy ion collisions, and thus provides a good probe of the density dependence of the symmetry energy [123,80]. Shown in Fig. 6 is the $t/{}^3\text{He}$ ratio as a function of cluster kinetic energy (in the center-of-mass system) from central collisions of ${}^{52}\text{Ca} + {}^{48}\text{Ca}$ at $E = 80$ MeV/nucleon by using the SBKD (left panel), MDYI (middle panel), and MDI (right panel) interactions with the soft (solid squares) and stiff (open squares) symmetry energies. Here, the soft (stiff) symmetry energy from the SBKD or MDYI interaction corresponds to the same density-dependent symmetry energy obtained from the MDI interaction with $x = 1(-2)$. For all cases, the free-space experimental NN cross sections are used. It is seen from Fig. 6 that for all nuclear interactions the ratio $t/{}^3\text{He}$ exhibits very different energy dependence for different symmetry energies. While the $t/{}^3\text{He}$ ratio decreases and/or increases weakly with kinetic energy for the stiff symmetry energy, it increases with kinetic energy for the soft symmetry energy. For both stiff and soft symmetry energies, the value of $t/{}^3\text{He}$ ratio is larger than that of the neutron to proton ratio of the whole reaction system, i.e., $N/Z = 1.5$, consistent with results from both experiments and the statistical model calculations for other reaction systems and incident energies [133, 134, 135, 136, 137].

It is interesting to note that for the isospin- and momentum-dependent MDI interaction, the $t/{}^3\text{He}$ ratio displays very different energy dependence for the soft and stiff symmetry energies, although their individual yields are not so sensitive to the density dependence of symmetry energy [123,80]. This is related to the different momentum-dependent symmetry potentials at different densities in the MDI interaction. Also, one can see from comparing Fig. 6 (a) and (b) that the momentum dependence of the isoscalar potential has obvious effects on the energy dependence of the $t/{}^3\text{He}$ ratio. These results indicate that the energy dependence of the $t/{}^3\text{He}$ ratio in heavy ion collisions induced by neutron-rich nuclei indeed provides a

sensitive probe of the isospin- and momentum-dependent single-nucleon potential in asymmetric nuclear matter.

4.2 Thermal properties of asymmetric nuclear matter

4.2.1 Temperature dependence of symmetry energy and symmetry free energy

While the exact knowledge on the symmetry energy at zero temperature is important for understanding ground state properties of exotic nuclei and properties of old neutron stars at β -equilibrium, the symmetry energy or symmetry free energy at finite temperature is important for determining the liquid-gas phase transition of asymmetric nuclear matter, the dynamical evolution of compact stars, and the explosion mechanisms of supernova [88,90,138,139,140,141,142,143,144].

For an asymmetric nuclear matter at thermal equilibrium with a finite temperature T , the nucleon phase space distribution function becomes the Fermi-Dirac distribution

$$f_{\tau}(\mathbf{r}, \mathbf{p}) = \frac{2}{h^3} \frac{1}{\exp\left(\frac{p^2/2m_{\tau} + U_{\tau} - \mu_{\tau}}{T}\right) + 1}, \quad (43)$$

where μ_{τ} is the chemical potential of proton or neutron and can be obtained from

$$\rho_{\tau} = \int f_{\tau}(\mathbf{r}, \mathbf{p}) d^3\mathbf{p}. \quad (44)$$

For fixed density ρ , isospin asymmetry δ , and temperature T , the chemical potential μ_{τ} and the nucleon distribution function $f_{\tau}(\mathbf{r}, \mathbf{p})$ can be determined numerically by a self-consistency iteration recipe [145,88]. The energy per nucleon $E(\rho, T, \delta)$ can then be obtained as

$$E(\rho, T, \delta) = \frac{1}{\rho} \left[V(\rho, T, \delta) + \sum_{\tau} \int d^3\mathbf{p} \frac{p^2}{2m_{\tau}} f_{\tau}(\mathbf{r}, \mathbf{p}) \right], \quad (45)$$

while the entropy per nucleon $S_{\tau}(\rho, T, \delta)$ is

$$S_{\tau}(\rho, T, \delta) = -\frac{8\pi}{\rho h^3} \int_0^{\infty} p^2 [n_{\tau} \ln n_{\tau} + (1 - n_{\tau}) \ln(1 - n_{\tau})] dp \quad (46)$$

with the occupation probability

$$n_{\tau} = \frac{1}{\exp\left(\frac{p^2/2m_{\tau} + U_{\tau} - \mu_{\tau}}{T}\right) + 1}. \quad (47)$$

Correspondingly, the free energy per nucleon $F(\rho, T, \delta)$ and the pressure $P(\rho, T, \delta)$ of the thermal equilibrium asymmetric nuclear matter can be obtained from the thermodynamic relations,

$$F(\rho, T, \delta) = E(\rho, T, \delta) - T \sum_{\tau} S_{\tau}(\rho, T, \delta), \quad (48)$$

$$P(\rho, T, \delta) = \sum_{\tau} \mu_{\tau} \rho_{\tau} - F(\rho, T, \delta) \rho. \quad (49)$$

As in the situation of zero temperature, phenomenological and microscopic studies [138, 139] have shown that the EOS of hot neutron-rich matter at density ρ , isospin asymmetry δ , and temperature T , can also be written as a parabolic function of δ , i.e.,

$$E(\rho, T, \delta) = E(\rho, T, \delta = 0) + E_{\text{sym}}(\rho, T)\delta^2 + \mathcal{O}(\delta^4). \quad (50)$$

The density- and temperature-dependent symmetry energy $E_{\text{sym}}(\rho, T)$ for hot neutron-rich matter can thus be extracted from $E_{\text{sym}}(\rho, T) \approx E(\rho, T, \delta = 1) - E(\rho, T, \delta = 0)$. Similarly, one can define the density and temperature dependent symmetry free energy $F_{\text{sym}}(\rho, T)$ by the following parabolic approximation to the free energy per nucleon:

$$F(\rho, T, \delta) = F(\rho, T, \delta = 0) + F_{\text{sym}}(\rho, T)\delta^2 + \mathcal{O}(\delta^4). \quad (51)$$

The above parabolic approximation to the free energy per nucleon has been shown to be a good approximation [88, 90], and this leads to $F_{\text{sym}}(\rho, T) \approx F(\rho, T, \delta = 1) - F(\rho, T, \delta = 0)$.

the eMDYI results with those from the MDI interaction, one can extract information about the effects of the momentum dependence of the symmetry potential, while the effects of the momentum dependence of the isoscalar part of the single-nucleon potential can be investigated by comparing the eMDYI results with those from the MID interaction.

For the MDI interaction, one can see from Fig. 7 that both the total symmetry energy $E_{\text{sym}}(\rho, T)$ and its potential energy part decrease with increasing temperature at all three considered densities. The kinetic contribution, on the other hand, increases slightly with increasing temperature at low temperatures and then decreases with increasing temperature at high temperatures for $\rho = 1.0\rho_0$ and $0.5\rho_0$, while it decreases monotonically for $\rho = 0.1\rho_0$. These features are uniquely determined by the isospin and momentum dependence in the MDI interaction. For MID and eMDYI interactions, the kinetic part of the total symmetry energy decreases with increasing temperature at all considered densities, while the potential part is independent of temperature and has the same value for the MID and eMDYI interactions. These results indicate that the temperature dependence of the total symmetry energy is due to both the potential and kinetic contributions for the MDI interaction, but it is only due to the kinetic contribution for the MID and eMDYI interactions.

The decrement of the kinetic energy part of the symmetry energy with temperature at very low densities is consistent with the results from the free Fermi gas model at high temperatures and/or very low densities [140, 146, 147, 141]. Also, the temperature dependence of the total symmetry energy $E_{\text{sym}}(\rho, T)$ is quite similar for all three interactions except that the MDI interaction displays a slightly stronger temperature dependence at higher temperatures. This is due to the fact that the nucleon phase-space distribution function varies self-consistently whether the single-nucleon potential is momentum dependent or not. As shown in Ref. [141], both the potential and kinetic parts of the symmetry energy $E_{\text{sym}}(\rho, T)$ also decrease with temperature for all considered densities when using the isospin- and momentum-dependent BGBD interaction. The different temperature dependence of the potential and kinetic parts of the symmetry energy between the MDI and BGBD interaction is due to the fact that the MDI and BGBD interactions have different forms for the energy density functional with the MDI interaction having a more complicated momentum dependence in the single-nucleon potential as mentioned earlier. This feature implies that the temperature dependence of the potential and kinetic parts of the symmetry energy depends on the isospin and momentum dependence of the in-medium nuclear effective interactions.

Experimentally, it is still a big challenge to determine the temperature dependence of the symmetry energy or symmetry free energy. It has been found both experimentally and theoretically that in many types of reactions the yield ratio $R_{21}(N, Z)$ of a fragment with proton number Z and neutron number N from two reactions reaching about the same temperature T respects an exponential

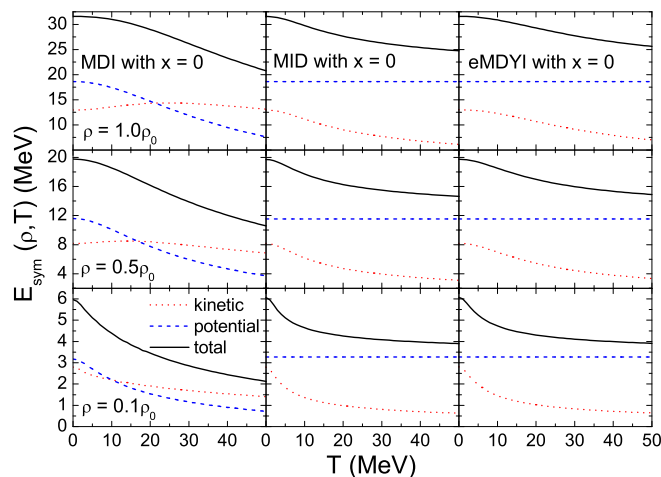


Fig. 7. (Color online) Total symmetry energy and its kinetic and potential parts as functions of temperature in MDI, MID, and eMDYI interactions with $x = 0$ at $\rho = 0.1\rho_0$, $0.5\rho_0$, and $1.0\rho_0$. Taken from Ref. [90].

Shown in Fig. 7 is the temperature dependence of the symmetry energy $E_{\text{sym}}(\rho, T)$ as well as its potential and kinetic energy parts in the MDI, MID, and eMDYI interactions with $x = 0$ at $\rho = 1.0\rho_0$, $0.5\rho_0$, and $0.1\rho_0$. The results are similar for other x values such as $x = -1$. We note that the MID interaction corresponds to the momentum-independent BKD energy density functional while the eMDYI interaction corresponds to the isoscalar momentum-dependent MDYI energy density functional but with their parameters refitted to the density-dependent EOS from the MDI interaction (See Ref. [88, 89, 90] for details). In the eMDYI interaction, the resulting single-nucleon potential is momentum dependent but its momentum dependence is isospin independent. Comparing

relationship $R_{21}(N, Z) \propto \exp(\alpha N)$ [148, 149, 150, 151, 152, 153, 154, 155, 156, 157, 158, 159]. In particular, it has been shown in several statistical and dynamical models under some assumptions [155, 156, 157] that the scaling coefficient α can be related to the symmetry energy $C_{\text{sym}}(\rho, T)$ via

$$\alpha = \frac{4C_{\text{sym}}(\rho, T)}{T} \Delta [(Z/A)^2], \quad (52)$$

where $\Delta[(Z/A)^2] \equiv (Z_1/A_1)^2 - (Z_2/A_2)^2$ is the $(Z/A)^2$ difference between the two fragmenting sources created in the two reactions. As pointed out in Ref. [140], because of the different assumptions used in the various derivations, the validity of Eq. (52) is still under debate as to whether and when the C_{sym} is actually the symmetry energy or the symmetry free energy. In addition, the physical interpretation for $C_{\text{sym}}(\rho, T)$ is also controversial, sometimes even contradictory, in the literature. The main issue is whether the C_{sym} measures the symmetry (free) energy of the fragmenting source or that of the fragments formed at freeze-out. This ambiguity also comes from the fact that the derivation of Eq. (52) is not unique. In particular, within the grand canonical statistical model for multifragmentation [155, 156], the C_{sym} is identified as the symmetry energy of primary fragments. While within the sequential Weisskopf model in the grand canonical limit [155], it refers to the symmetry energy of the emission source. Following the arguments in Ref. [140], we assume here that the C_{sym} reflects the symmetry energy of *bulk nuclear matter* for the emission source.

The temperature dependence of the symmetry energy has been studied based on a simplified degenerate Fermi gas model [140], and it was shown that the experimentally observed decrease of the symmetry energy with the increasing excitation energy or centrality in isotopic scaling analyses of heavy ion collisions can be well understood analytically within the degenerate Fermi gas model. In particular, it was found that the evolution of the symmetry energy extracted from the isotopic scaling analysis is mainly due to the variation in the freeze-out density rather than the temperature when fragments are emitted in the reactions.

Shown in Fig. 8 is the symmetry energy $E_{\text{sym}}(\rho, T)$ and symmetry free energy $F_{\text{sym}}(\rho, T)$ as functions of temperature using the more realistic MDI interaction with $x = 0$ and -1 at different densities from $0.1\rho_0$ to ρ_0 . One can see that while the symmetry energy $E_{\text{sym}}(\rho, T)$ decreases slightly with increasing temperature at a given density, the symmetry free energy $F_{\text{sym}}(\rho, T)$ increases instead. Around the saturation density ρ_0 , the difference between the symmetry energy $E_{\text{sym}}(\rho, T)$ and the symmetry free energy $F_{\text{sym}}(\rho, T)$ is quite small compared with their values at $T = 0$ MeV. This feature supports the assumption on identifying $C_{\text{sym}}(\rho, T)$ to $E_{\text{sym}}(\rho, T)$ at lower temperatures and not so low densities [149, 150, 151]. On the other hand, the symmetry free energy $F_{\text{sym}}(\rho, T)$ at low densities displays a stronger temperature dependence, and it is significantly larger than the symmetry energy $E_{\text{sym}}(\rho, T)$ at moderate and high temperatures. This can be understood from the fact that the entropy contribution to the

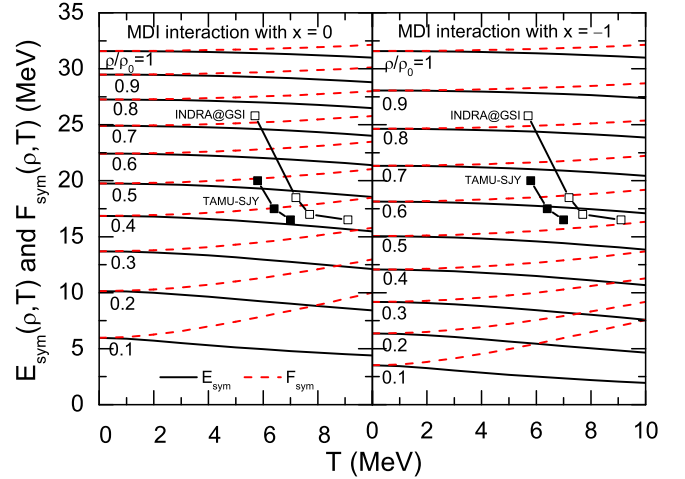


Fig. 8. (Color online) Temperature dependence of the symmetry energy (solid lines) and symmetry free energy (dashed lines) using MDI interaction with $x = 0$ (left panel) and -1 (right panel) at different densities from $0.1\rho_0$ to ρ_0 . The experimental data from Texas A&M University (solid squares) and the INDRA-ALADIN collaboration at GSI (open squares) are included for comparison. Taken from Ref. [88].

symmetry free energy $F_{\text{sym}}(\rho, T)$ becomes important at low densities. We would like to point out that the entropy and thus the symmetry free energy at low densities are affected strongly by the formation of clusters [154, 160, 161, 162], which are not considered here in the mean-field calculations.

4.2.2 Liquid-gas phase transition of asymmetric nuclear matter

The feature of short-range repulsion and long-range attraction in the nucleon-nucleon interaction has led to the expectation that the liquid-gas (LG) phase transition should also exist in nuclear matter. Since the early work, see, e.g., Refs. [163, 164, 165, 166], a lot of studies have been devoted to investigating the properties of the nuclear LG phase transition both experimentally and theoretically during the past three decades (see, e.g., Refs. [167, 168, 169] for a recent review). Most of these investigations focused on studying features of the LG phase transition in symmetric nuclear matter. Theoretically, new features of the LG phase transition in isospin asymmetric nuclear matter are expected. In particular, because of the two conserved charges of baryon number and isospin due to the two components of protons and neutrons in an asymmetric nuclear matter, the LG phase transition has been suggested to be of second order [170]. Since the isovector nuclear interaction and the density dependence of the nuclear symmetry energy play a central role in understanding the thermal properties of asymmetric nuclear matter [169, 1, 2], it is therefore of great interest to investigate how the isospin and momentum dependence of the nuclear effective in-

interactions affect the LG phase transition in asymmetric nuclear matter.

According to the Gibbs conditions for the phase coexistence of the LG phase transition, the two-phase coexistence equations in hot asymmetric nuclear matter can be expressed as

$$P^L(T, \rho^L, \delta^L) = P^G(T, \rho^G, \delta^G), \quad (53)$$

$$\mu_n^L(T, \rho^L, \delta^L) = \mu_n^G(T, \rho^G, \delta^G), \quad (54)$$

$$\mu_p^L(T, \rho^L, \delta^L) = \mu_p^G(T, \rho^G, \delta^G), \quad (55)$$

where L (G) stands for the liquid (gas) phase. The Gibbs phase equilibrium conditions require equal pressures and chemical potentials for two phases with different densities and isospin asymmetries. For a fixed pressure, the two solutions form the edges of a rectangle in the neutron and proton chemical potential isobars as a function of isospin asymmetry δ , and this can be found through the geometrical construction method [170, 171, 89]. For each interaction, the two different values of δ correspond to two different phases with different densities, and the higher density phase (with smaller δ value) defines the liquid phase while the lower density phase (with larger δ value) defines the gas phase. The binodal surface then can be obtained with all such pairs of $\delta(T, P)$ and $\delta'(T, P)$.

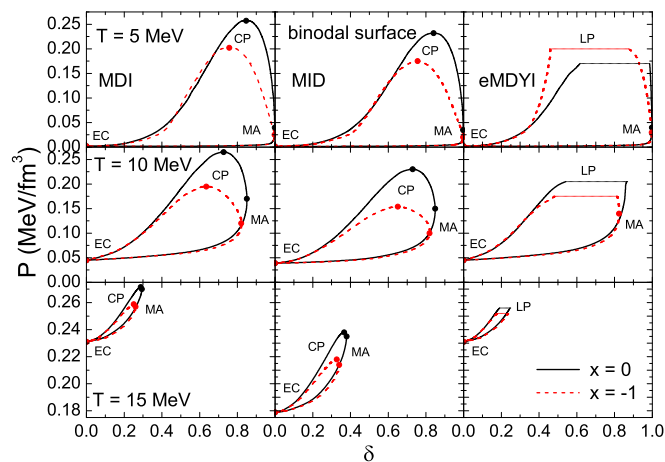


Fig. 9. (Color online) The section of binodal surface at $T = 5, 10,$ and 15 MeV in the P - δ plane from the MDI, MID, and eMDYI interactions with $x = 0$ and $x = -1$. Taken from Ref. [90].

Shown in Fig. 9 is the section of binodal surface at $T = 5, 10,$ and 15 MeV in the P - δ plane from the MDI, MID, and eMDYI interactions with $x = 0$ and $x = -1$. The critical pressure (CP) and the limiting pressure (LP) as well as the equal concentration (EC) and the maximal asymmetry (MA) points are also indicated in Fig. 9. One can see that for the MDI and MID interactions the binodal surface has a critical pressure, while for the eMDYI interaction the binodal surface is cut off by a limit pressure which is due to the specific momentum dependence in the eMDYI interaction as discussed in Ref. [89]. There

is no phase-coexistence region above the critical pressure or below the pressure of equal concentration point. Moreover, the right side of the binodal surface is the region of gas phase while the left side is the region of liquid phase, and the inside of the surface corresponds to the phase-coexistence region.

It is seen from Fig. 9 that the stiffness of the symmetry energy significantly affects the critical pressure, with a softer symmetry energy ($x = 0$) giving a higher critical pressure and a larger area of phase-coexistence region. For the limit pressure from the eMDYI interaction, this holds true at $T = 10$ MeV and $T = 15$ MeV, but the opposite result is observed at $T = 5$ MeV. Comparing the results from the MDI interaction to those from the MID interactions, one can see that the isospin and momentum dependence of the nuclear effective interaction in the MDI interaction seems to increase the critical pressure by a larger amount. In addition, at $T = 5$ MeV and $T = 10$ MeV, the area of phase-coexistence region for the MID interaction is smaller than that for the MDI interaction, but the opposite result is obtained at $T = 15$ MeV.

4.2.3 Differential isospin fractionation

As pointed out above, the lower density gas phase is more neutron-rich than the coexisting liquid phase. This feature leads to the so-called isospin fractionation (IsoF) phenomenon that has been observed in heavy ion reaction experiments, see, e.g., Ref. [172]. The nonequal partition of the system's isospin asymmetry, i.e., the IsoF, has been found to be a general phenomenon in essentially all thermodynamical models and transport model simulations of heavy ion collisions (see, e.g., Refs. [8, 167, 168, 5] for reviews).

In almost all existing theoretical and experimental studies on IsoF in the literature, only the ratio between all neutrons and protons in the liquid or the gas phase was considered, which is normally referred to as the integrated IsoF. On the other hand, it has been shown [173] that completely new and very interesting physics can be revealed from the differential IsoF that takes consideration of the nucleon momentum dependence of the neutron/proton ratio in the liquid or the gas phase. For energetic nucleons, with their differential IsoF very sensitive to the momentum dependence of the symmetry potential, the nucleon phase-space distribution function f_τ can be well approximated by the Boltzmann distribution. For these nucleons in either the liquid (L) or gas (G) phase, the neutron/proton ratio can be expressed as

$$(n/p)_{L/G} = \exp[-(E_n^{L/G} - E_p^{L/G} - \mu_n^{L/G} + \mu_p^{L/G})/T]. \quad (56)$$

The energy difference of neutrons and protons having the same kinetic energy and mass, i.e.,

$$E_n^{L/G} - E_p^{L/G} = U_n^{L/G} - U_p^{L/G} \approx 2\delta_{L/G} \cdot U_{\text{sym}}(p, \rho_{L/G}) \quad (57)$$

is directly linked to the symmetry potential U_{sym} . Because of the chemical equilibrium conditions given in Eqs. (54)

and (55), the chemical potentials cancel out exactly in the double neutron/proton ratio and this leads to

$$\frac{(n/p)_G}{(n/p)_L}(p) = \exp[-2(\delta_G \cdot U_{\text{sym}}(p, \rho_G) - \delta_L \cdot U_{\text{sym}}(p, \rho_L))/T]. \quad (58)$$

This general expression clearly indicates that the differential IsoF for energetic nucleons can carry direct information on the momentum dependence of the symmetry potential.

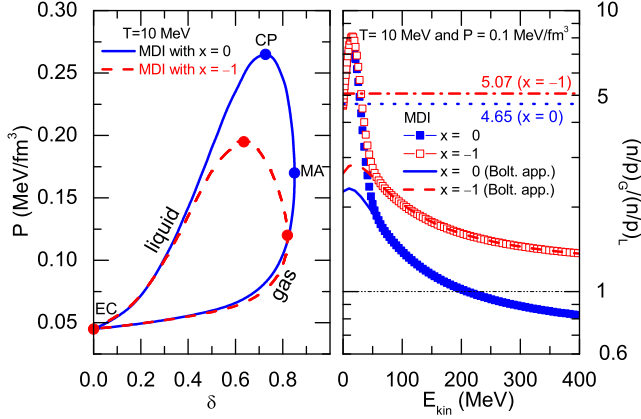


Fig. 10. (Color online) Left window: the section of binodal surface at $T = 10$ MeV from the MDI interaction with $x = 0$ and $x = -1$. Right window: the double neutron/proton ratio in the gas and liquid phases $(n/p)_G/(n/p)_L$ as a function of the nucleon kinetic energy. Taken from Ref. [173].

As an example, a typical section of the binodal surface at $T = 10$ MeV is shown in the left window of Fig. 10 using the MDI interaction with $x = 0$ and $x = -1$. The integrated IsoF phenomenon with a more neutron-rich gas phase is clearly observed. Moreover, one can see that the stiffer symmetry energy ($x = -1$) significantly lowers the critical point (CP). When the pressure is less than than about $P = 0.12$ MeV/fm³, the magnitude of the integrated IsoF becomes, however, essentially independent of the stiffness of the symmetry energy.

To demonstrate the advantages of the differential IsoF analyses over the integrated ones, we study the differential IsoF at $T = 10$ MeV and $P = 0.1$ MeV/fm³ for which the integrated IsoF is essentially independent of the x parameter as seen in the left window of Fig. 10. Shown in the right window of Fig. 10 are the double neutron/proton ratios in the gas and liquid phases $\frac{(n/p)_G}{(n/p)_L}(p)$ as a function of nucleon momentum or kinetic energy, i.e., the differential IsoFs, for both $x = 0$ and $x = -1$ in the MDI interaction. Interestingly, one can see that the double neutron/proton ratios in both cases exhibit a strong momentum dependence. In addition, while the integrated double neutron/proton ratios of 4.65 ($x = 0$) and 5.07 ($x = -1$) are very close to each other, the differential IsoF for nucleons with kinetic energies higher than about 50 MeV is very sensitive to the x values used for the density dependence of the symmetry energy. Furthermore, it is surprising to

see that the IsoF for $x = 0$ becomes less than one for nucleons with kinetic energies higher than about 220 MeV, and this means there are more energetic neutrons than protons in the liquid phase compared to the gas phase.

Experimentally, it could be a big challenge to measure the differential IsoF because the momentum distribution of the neutron/proton ratio in the liquid phase may not be directly measured since only free nucleons and bound nuclei in their ground states at the end of the collisions can be detected in heavy ion collisions. Nevertheless, precursors and/or residues of the effects due to the differential IsoF may still be detectable in heavy ion collisions induced by radioactive beams [173]. While it may be very challenging to test experimentally the predictions of the differential IsoF, future comparisons with experimental data will allow us to extract critical information on the nuclear symmetry potential, especially its momentum dependence, and thus give deeper insight on the isospin- and momentum-dependent effective interactions.

4.3 The inner edge of neutron star crust

Neutron stars provide an excellent site to explore the properties of nuclear matter at extreme isospin conditions and thus become an important astrophysical laboratory to investigate the isospin- and momentum-dependent in-medium nuclear effective interactions. In the present section, we highlight some results obtained with the MDI interaction on the location of the inner edge of neutron star crust. The latter separates the liquid core from the inner crust in neutron stars, and it plays an important role in determining the structural properties of neutron stars such as the crustal fraction of total moment of inertia and the mass-radius relations of static neutron stars [3].

The transition density ρ_t at the inner edge of neutron star crust can be determined from comparing relevant properties of the nonuniform solid crust and the uniform liquid core. This is, however, very difficult in practice since the inner crust may contain the so-called “nuclear pasta” with very complicated geometries [3, 174, 175, 176, 177]. A good approximation used in the determination of ρ_t is to search for the density at which the uniform liquid first becomes unstable against small amplitude density fluctuations with clusterization. This approximation has been shown to give a very small error for the actual core-crust transition density, and it would produce the exact transition density for a second-order phase transition [178, 179, 180, 181]. In the literature, several such methods, including the thermodynamical method [182, 183, 184], the dynamical curvature matrix method [178, 179, 185, 186, 187, 188, 189], the Vlasov equation method [167, 190, 191, 192, 193], and the random phase approximation (RPA) [194, 181, 191], have been used extensively. Once the ρ_t is determined, one can easily obtain the pressure P_t at the inner edge, which is also an important quantity and might be measurable indirectly from observations of pulsar glitches [183, 195]. In the following, we briefly introduce the dynamical (curvature matrix) method and present some results obtained with this method.

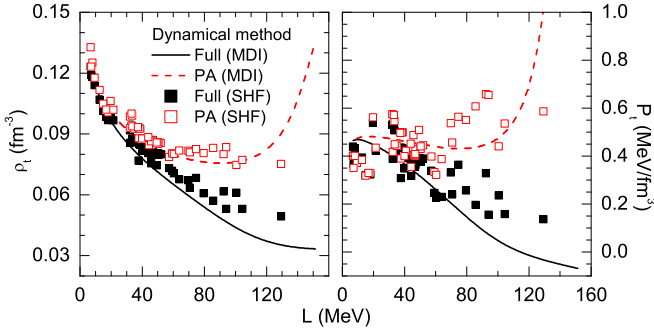


Fig. 11. (Color online) The transition density ρ_t (left panel) and the corresponding pressure P_t (right panel) as functions of symmetry energy slope parameter L by using the dynamical methods with the full EOS and its parabolic approximation (PA). The MDI (curves) and Skyrme (squares) interactions are used. The calculated results are taken from Refs. [47,48].

In the dynamical method, a homogeneous npe matter will be stable against small periodic density perturbations with clusterization if the following condition can be satisfied [178,185,186,187,188]

$$V_{\text{dyn}}(k) = V_0 + \beta k^2 + \frac{4\pi e^2}{k^2 + k_{TF}^2} > 0, \quad (59)$$

with

$$V_0 = \frac{\partial \mu_p}{\partial \rho_p} - \frac{(\partial \mu_n / \partial \rho_p)^2}{\partial \mu_n / \partial \rho_n}, \quad k_{TF}^2 = \frac{4\pi e^2}{\partial \mu_e / \partial \rho_e},$$

$$\beta = D_{pp} + 2D_{np}\zeta + D_{nn}\zeta^2, \quad \zeta = -\frac{\partial \mu_n / \partial \rho_p}{\partial \mu_n / \partial \rho_n}.$$

In the above expressions, μ_i is the chemical potential of particle i and k is the wavevector of the spatially periodic density perturbations. The three terms in Eq. (59) represent the contributions from the bulk nuclear matter, the density gradient (surface) terms, and the Coulomb interaction, respectively. $D_{np} = D_{pn}$ and $D_{pp} = D_{nn}$ are coefficients of density gradient terms. The $V_{\text{dyn}}(k)$ has the minimal value of $V_{\text{dyn}}(k_{\text{min}}) = V_0 + 2(4\pi e^2 \beta)^{1/2} - \beta k_{TF}^2$ at $k_{\text{min}} = [(4\pi e^2 / \beta)^{1/2} - k_{TF}^2]^{1/2}$ [185,186,187,178,188]. The density at which $V_{\text{dyn}}(k_{\text{min}})$ vanishes then corresponds to the ρ_t .

Shown in Fig. 11 are the ρ_t and the corresponding P_t as functions of the slope parameter L of the symmetry energy using the dynamical methods with the MDI interaction by varying x and 51 Skyrme forces (See Ref. [48] for the details of the 51 Skyrme forces). For comparisons, we have included results with the full EOS and its parabolic approximation (PA), i.e., $E(\rho, \delta) = E(\rho, \delta = 0) + E_{\text{sym}}(\rho)\delta^2 + O(\delta^4)$ from the same MDI interaction and Skyrme forces. For the MDI interaction, which does not have gradient terms in its present form, the coefficients of density gradient terms have been assumed to be $D_{pp} = D_{nn} = D_{np} = 132 \text{ MeV} \cdot \text{fm}^5$, which are consistent with the Skyrme-Hartree-Fock calculations [188,47]. With the full EOS, it is clearly seen that the ρ_t and P_t decrease quickly with increasing

L for both MDI and Skyrme interactions with the former giving lower values than the latter. On the other hand, it is very surprising to see that the PA drastically changes the results, especially for stiffer symmetry energies (i.e., larger L values). Actually, the large error introduced by the PA can be understood from the fact that the β -stable npe matter is usually highly neutron-rich and the higher-order δ term contribution is appreciable. This is especially true for the stiffer symmetry energy (i.e., larger L values) which generally gives rise to a more neutron-rich npe matter at subsaturation densities. In addition, since the energy curvatures are involved in the stability conditions, the contributions from higher-order terms in the EOS are thus multiplied by a larger factor than the quadratic term [47,48]. These features are in agreement with the early finding [196] that the ρ_t is very sensitive to the details of the nuclear EOS.

The above results indicate that to determine the ρ_t and P_t , one may introduce a big error by assuming *a priori* that the EOS of asymmetric nuclear matter is parabolic in δ for a given interaction. Therefore, the ρ_t - L and P_t - L correlation obtained with the full EOS should be used to constrain the ρ_t and P_t from the experimentally constrained L values. From Fig. 11, one can obtain $\rho_t \approx 0.075 \pm 0.015 \text{ fm}^{-3}$ and $P_t \approx 0.37 \pm 0.17 \text{ MeV/fm}^3$ if one assumes a constraint of $L = 50 \pm 20 \text{ MeV}$ which probably represents our present best knowledge on the L parameter [197]. The present results also demonstrate that the isospin- and momentum-dependent effective interactions play a critically important role in determining the core-crust transition density ρ_t and the corresponding pressure P_t in neutron stars.

It should be mentioned that the isospin- and momentum-dependent effective interactions may also significantly affect the critical density above which the proton fraction is larger than about 1/9 so as to trigger the direct URCA process that can lead to a faster cooling of neutron stars [198]. From Fig. 2 of Ref. [48], we find that the critical density of the direct URCA process is about 0.25 (0.55) fm^{-3} for the MDI interaction with $x = -1$ ($x = 0$). Furthermore, the central density of a neutron star with canonical mass of $1.4M_\odot$ is found to be about 0.42 (0.57) fm^{-3} for the MDI interaction with $x = -1$ ($x = 0$). These results imply that the direct URCA process may occur in a neutron star with canonical mass of $1.4M_\odot$ for the MDI interaction with $x = -1$ and $x = 0$.

5 Extension of the MDI interaction

While the MDI interaction has been extensively applied in transport model simulations of heavy ion collisions as well as the investigations of thermal properties of asymmetric nuclear matter and neutron stars, some studies have also been performed to extend and improve the MDI interaction in recent years. In this section, we review the extended MDI interaction [199] for the baryon octet and its application to hybrid stars as well as the improved MDI interaction [71] with separate density-dependent terms for neutrons and protons to take into account more accurately

the effect of the isospin dependence of in-medium many-body forces.

5.1 The extended MDI interaction for the baryon octet

During the past decades, significant progress has been made in understanding the in-medium effective NN interaction. In contrast, the nucleon-hyperon (NY) and hyperon-hyperon (YY) interactions in nuclear medium are poorly known. The latter is important for understanding a number of important issues in nuclear physics and astrophysics, such as the properties of hypernuclei, the production of strange hadrons in high energy heavy ion collisions, the EOS of dense baryonic matter, and the properties of neutron stars that may have abundant hyperons in their interiors. Therefore, it is of great importance to develop an effective model for the NY and YY interactions in nuclear medium. In the following, we review the work on extending the MDI interaction to include NY and YY interactions [199].

5.1.1 The extended MDI interaction

In the extended MDI interaction [199], the NY and YY interactions have been assumed to have the same density and momentum dependence as the interactions between two nucleons in the MDI interaction. The potential energy density of a hypernuclear matter due to interactions between any two octet baryons then has the following form:

$$V_{bb'} = \sum_{\tau_b, \tau_{b'}} \left[\frac{A_{bb'}}{2\rho_0} \rho_{\tau_b} \rho_{\tau_{b'}} + \frac{A'_{bb'}}{2\rho_0} \tau_b \tau_{b'} \rho_{\tau_b} \rho_{\tau_{b'}} \right. \\ \left. + \frac{B_{bb'}}{\sigma + 1} \frac{\rho^{\sigma-1}}{\rho_0^\sigma} (\rho_{\tau_b} \rho_{\tau_{b'}} - x \tau_b \tau_{b'} \rho_{\tau_b} \rho_{\tau_{b'}}) \right. \\ \left. + \frac{C_{\tau_b, \tau_{b'}}}{\rho_0} \int \int d^3 \mathbf{p} d^3 \mathbf{p}' \frac{f_{\tau_b}(\mathbf{r}, \mathbf{p}) f_{\tau_{b'}}(\mathbf{r}, \mathbf{p}')}{1 + (\mathbf{p} - \mathbf{p}')^2 / \Lambda^2} \right], \quad (60)$$

where b (b') denotes the baryon octet, i.e., N , Λ , Σ , and Ξ . We use the conventions that $\tau_N = -1$ for neutron and 1 for proton (Note: this is opposite to the convention used earlier), $\tau_\Lambda = 0$ for Λ , $\tau_\Sigma = -1$ for Σ^- , 0 for Σ^0 and 1 for Σ^+ , and $\tau_\Xi = -1$ for Ξ^- and 1 for Ξ^0 . In the above, the total baryon density is then given by $\rho = \sum_b \sum_{\tau_b} \rho_{\tau_b}$, and $f_{\tau_b}(\mathbf{r}, \mathbf{p})$ is the phase-space distribution function of particle species τ_b . The $A_{bb'}$, $A'_{bb'}$, $B_{bb'}$, and $C_{\tau_b, \tau_{b'}}$ are interaction parameters. If there are only nucleons, one can rewrite $A_{NN} = (A_l + A_u)/2$, $A'_{NN} = (A_l - A_u)/2$, $B_{NN} = B$, and $C_{\tau_N, \tau'_N} = C_l$ for $\tau_N = \tau'_N$ and $C_{\tau_N, \tau'_N} = C_u$ for $\tau_N \neq \tau'_N$, which then reduce to the original parameters in the MDI interaction for nucleons [69,70]. Again, the parameter x is used here to model the isospin effect on the interaction energy in hypernuclear matter.

The single-particle potential for a baryon of species τ_b in a hypernuclear matter can then be obtained from the

total potential energy density of the hypernuclear matter, given by $V_{HP} = (1/2) \sum_{b, b'} V_{bb'}$, as

$$U_{\tau_b}(p) = \frac{\delta}{\delta \rho_{\tau_b}} V_{HP} \\ = \sum_{b'(b' \neq b)} \sum_{\tau_{b'}} \left[\frac{A_{bb'}}{2\rho_0} \rho_{\tau_{b'}} + \frac{A'_{bb'}}{2\rho_0} \tau_b \tau_{b'} \rho_{\tau_{b'}} \right. \\ \left. + \frac{B_{bb'}}{\sigma + 1} \frac{\rho^{\sigma-1}}{\rho_0^\sigma} (\rho_{\tau_{b'}} - x \tau_b \tau_{b'} \rho_{\tau_{b'}}) + \frac{C_{\tau_b, \tau_{b'}}}{\rho_0} \right. \\ \left. \times \int d^3 \mathbf{p}' \frac{f_{\tau_{b'}}(\mathbf{r}, \mathbf{p}')}{1 + (\mathbf{p} - \mathbf{p}')^2 / \Lambda^2} \right] + \sum_{\tau'_b} \left[\frac{A_{bb'}}{\rho_0} \rho_{\tau'_b} \right. \\ \left. + \frac{A'_{bb'}}{\rho_0} \tau_b \tau'_b \rho_{\tau'_b} + \frac{2B_{bb'}}{\sigma + 1} \frac{\rho^{\sigma-1}}{\rho_0^\sigma} (\rho_{\tau'_b} - x \tau_b \tau'_b \rho_{\tau'_b}) \right. \\ \left. + \frac{2C_{\tau_b, \tau'_b}}{\rho_0} \int d^3 \mathbf{p}' \frac{f_{\tau'_b}(\mathbf{r}, \mathbf{p}')}{1 + (\mathbf{p} - \mathbf{p}')^2 / \Lambda^2} \right] \\ \left. + \sum_{b', b''} \left[B_{b' b''} \frac{\sigma - 1}{\sigma + 1} \frac{\rho^{\sigma-2}}{\rho_0^\sigma} \right. \right. \\ \left. \left. \times \sum_{\tau_b} \sum_{\tau_{b''}} (\rho_{\tau_b} \rho_{\tau_{b''}} - x \tau_b \tau_{b''} \rho_{\tau_b} \rho_{\tau_{b''}}) \right]. \quad (61)$$

The parameters $A_{bb'}$, $A'_{bb'}$, $B_{bb'}$, and $C_{\tau_b, \tau_{b'}}$ for NY and YY interactions can in principle be determined from the free space NY and YY interactions. Due to the lack of NY scattering experiments, knowledge on the NY interactions has been mainly obtained from the hyperon single-particle potentials extracted empirically from analyzing Λ [200] as well as Σ [201,202] and Ξ [203] production in nuclear reactions. Although the NY interaction has been extensively studied in the past [204,205,206], the isospin and momentum dependence of the in-medium NY interactions are still not well determined, and the situation is even worse for YY interactions. In the extended MDI interaction, the parameters $A_{bb'}$, $A'_{bb'}$, $B_{bb'}$, and $C_{\tau_b, \tau_{b'}}$ are thus assumed to be proportional to corresponding ones in the NN interaction. Particularly, for $A_{bb'}$, $A'_{bb'}$, and $B_{bb'}$, one has

$$A_{bb'} = f_{bb'} A_{NN}, \\ A'_{bb'} = f_{bb'} A'_{NN}, \\ B_{bb'} = f_{bb'} B_{NN}, \quad (62)$$

and for $C_{\tau_b, \tau_{b'}}$, one has

$$C_{\tau_b, \tau_{b'}} = \begin{cases} f_{bb'} \frac{C_l + C_u}{2} & (\tau_b \text{ or } \tau_{b'} = 0), \\ f_{bb'} C_l & (\tau_b = \tau_{b'} \neq 0), \\ f_{bb'} C_u & (\tau_b \neq \tau_{b'} \neq 0), \end{cases}$$

with hyperons Λ and Σ^0 treated differently.

The values of $f_{bb'}$ are determined by fitting the empirical potential $U_b^{(b')}$ of baryon b at rest in a medium consisting of baryon species b' . For hyperons in symmetric nuclear matter at saturation density, their potentials are

$$U_\Lambda^{(N)}(\rho_N = \rho_0) = -30 \text{ MeV} \quad (63)$$

Table 1. Parameters for the MDI-Hyp-A and MDI-Hyp-R interactions with $x = 0$ and $x = -1$. All except σ are in units of MeV. $A'_{N\Sigma}(R)$ and $B_{N\Sigma}(R)$ are for the MDI-Hyp-R interaction, and $A'_{N\Sigma}(A)$ and $B_{N\Sigma}(A)$ are for the MDI-Hyp-A interaction. Other parameters are the same for both interactions. Taken from Ref. [199].

A_{NN}	A_{NA}	$A_{N\Sigma}$	$A_{N\Xi}$	$A_{\Lambda\Lambda}$	$A_{\Lambda\Sigma}$	$A_{\Lambda\Xi}$	$A_{\Sigma\Sigma}$	$A_{\Sigma\Xi}$	$A_{\Xi\Xi}$	Λ	σ
-108.28	-108.28	-108.28	-79.04	-68.21	-135.34	-135.34	-53.05	-108.28	-57.39	263.04	4/3
x	A'_{NN}	$A'_{N\Sigma}(A)$	$A'_{N\Sigma}(R)$	$A'_{N\Xi}$	$A'_{\Sigma\Sigma}$	$A'_{\Sigma\Xi}$	$A'_{\Xi\Xi}$				
0	-12.29	-12.29	-28.65	-8.98	-6.02	-12.29	-6.52				
-1	-103.45	-103.45	-241.04	-75.52	-50.69	-103.45	-54.83				
B_{NN}	B_{NA}	$B_{N\Sigma}(A)$	$B_{N\Sigma}(R)$	$B_{N\Xi}$	$B_{\Lambda\Lambda}$	$B_{\Lambda\Sigma}$	$B_{\Lambda\Xi}$	$B_{\Sigma\Sigma}$	$B_{\Sigma\Xi}$	$B_{\Xi\Xi}$	
106.35	106.35	106.35	247.80	77.64	67.00	132.94	132.94	52.11	106.35	56.37	
C_{τ_N, τ_N}	$C_{\tau_N, -\tau_N}$	C_{τ_N, τ_Σ}	$C_{\tau_N, -\tau_\Sigma}$	C_{τ_N, τ_Ξ}	$C_{\tau_N, -\tau_\Xi}$	$C_{\tau_\Sigma, \tau_\Sigma}$	$C_{\tau_\Sigma, -\tau_\Sigma}$	$C_{\tau_\Sigma, \tau_\Xi}$	$C_{\tau_\Sigma, -\tau_\Xi}$	C_{τ_Ξ, τ_Ξ}	$C_{\tau_\Xi, -\tau_\Xi}$
-11.70	-103.40	-11.70	-103.40	-8.54	-75.48	-5.73	-50.67	-11.70	-103.40	-6.20	-54.80
C_{NA}	$C_{N\Sigma^0}$	$C_{\Lambda\Lambda}$	$C_{\Lambda\Sigma}$	$C_{\Lambda\Xi}$	$C_{\Sigma^0\Sigma}$	$C_{\Sigma^0\Xi}$					
-57.55	-57.55	-36.26	-71.94	-71.94	-28.20	-57.55					

for the Λ potential from the analysis of (π^+, K^+) and (K^-, π^-) reactions [207, 208] and

$$U_{\Xi}^{(N)}(\rho_N = \rho_0) = -18 \text{ MeV} \quad (64)$$

for the Ξ potential from the analysis of $(\Xi, {}^4_{\Lambda}H)$ [209] and (K^-, K^+) [210, 211] reactions. This leads to $f_{NA} = 1$ and $f_{N\Xi} = 0.73$. For the Σ hyperon, its potential in symmetric nuclear matter at saturation density was taken to be attractive in earlier studies [201], but more recent analysis indicate that it should be repulsive [212, 213, 214, 215, 216]. To take into account these uncertainties, both the attractive and repulsive cases

$$U_{\Sigma}^{(N)}(\rho_N = \rho_0) = \pm 30 \text{ MeV} \quad (65)$$

have therefore been considered in Ref. [199]. By setting $f_{N\Sigma} = 1$ one obtains an attractive ΣN interaction, called MDI-Hyp-A in the following. To get a repulsive ΣN interaction, called MDI-Hyp-R in the following, one can adjust the values of positive and negative terms in the single-particle potential by setting $B_{N\Sigma} = 2.33B_{NN}$ and $A'_{N\Sigma} = 2.33A'_{NN}$ but keeping other parameters as in the MDI-Hyp-A interaction. A similar method of changing an attractive ΣN interaction to a repulsive one was used in the relativistic mean-field model calculation [217] by adjusting the coupling constants of ω and ρ mesons.

For the YY interaction, the parameters are determined according to [218]

$$U_Y^{(Y')}(\rho_{Y'} = \rho_0) \sim -40 \text{ MeV}, \quad (66)$$

which leads to $f_{\Lambda\Lambda} = 0.63$, $f_{\Lambda\Sigma} = 1.25$, $f_{\Lambda\Xi} = 1.25$, $f_{\Sigma\Sigma} = 0.49$, $f_{\Sigma\Xi} = 1$, and $f_{\Xi\Xi} = 0.53$ for the strength of the YY interactions.

For completeness, we list the detailed parameter values of the MDI-Hyp-A and MDI-Hyp-R interactions with $x = 0$ and $x = -1$ in Table. 1. These parameterizations can be considered as a baseline for studying the properties of hypernuclear matter, and more sophisticated treatments can be made in future after the in-medium properties of hyperons are better understood.

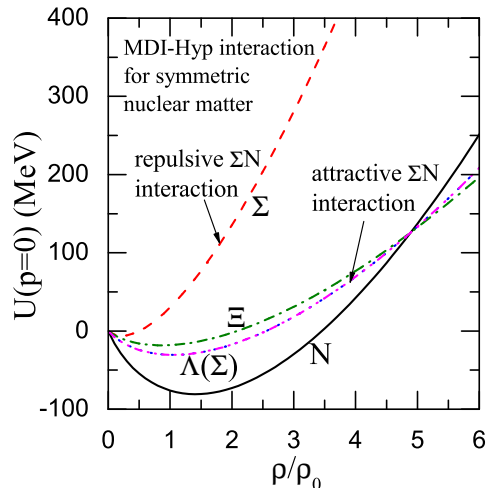


Fig. 12. (Color online) Density dependence of single-particle potentials for particles at rest in symmetric nuclear matter. Taken from Ref. [199].

5.1.2 Single-particle potentials for the baryon octet in asymmetric nuclear matter

The single-particle potential as given by Eq. (61) is an important quantity linked to the interaction of a particle in nuclear medium. Shown in Fig. 12 is the density dependence of the single-particle potential of a particle at rest in symmetric nuclear matter. One can see that, although the nucleon potential is more attractive at saturation density ρ_0 than those of hyperons, it becomes more repulsive than the hyperon potentials above about $5\rho_0$, including the Σ potential with MDI-Hyp-A. For the Σ potential with MDI-Hyp-R, it becomes more repulsive with increasing density and becomes weakly attractive only at very low densities. Compared with results from other models given in Ref. [219] (and references therein), the single-particle potentials of Λ and Σ presented here are close to those from the chiral EFT [220], but more repulsive than those from the G-matrix calculations within the soft core

Nijmegen model or the Jülich meson-exchange model for the free NY interactions, specially at high densities.

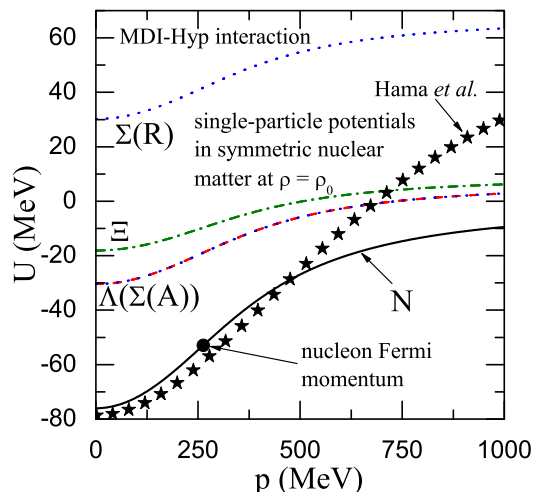


Fig. 13. (Color online) Single-particle potentials in symmetric nuclear matter at saturation density ρ_0 as functions of particle momentum. The Schrödinger equivalent potential obtained by Hama *et al.* [221,222] from the nucleon-nucleus scattering data is shown by stars for comparison. $\Sigma(A)$ and $\Sigma(R)$ are for the MDI-Hyp-A and MDI-Hyp-R interactions, respectively. Taken from Ref. [199].

In the extended MDI interaction, the single-particle potential of a particle is also momentum dependent. Shown in Fig. 13 is the single-particle potential as a function of the particle momentum for both nucleons and hyperons in symmetric nuclear matter at saturation density ρ_0 . Again, results for Σ potential with both MDI-Hyp-A and MDI-Hyp-R interactions are shown for comparison. Also indicated in Fig. 13 is the nucleon Fermi momentum. One can see that the nucleon single-particle potential from the MDI interaction is consistent with the Schrödinger equivalent potential obtained by Hama *et al.* from Dirac phenomenology of the nucleon-nucleus scattering data [221,222] up to the nucleon momentum of 500 MeV. For hyperons, their single-particle potentials from the extended MDI interaction agree with that obtained from the G-matrix calculations with the free Nijmegen NY interaction [223] at low momenta since both are constrained by available experimental data. However, they are slightly different at high momenta. Therefore, the momentum dependence of NY and YY interactions remains an open question, especially at high momenta. In addition, the density dependence of the single-particle potential for high momentum particles is poorly known.

For the extended MDI interaction, similarly to the case of nucleons, the single-particle potentials of Σ and Ξ in asymmetric nuclear matter are also approximately linear in the isospin asymmetry δ of the matter. The single-particle potential of a particle in asymmetric nuclear mat-

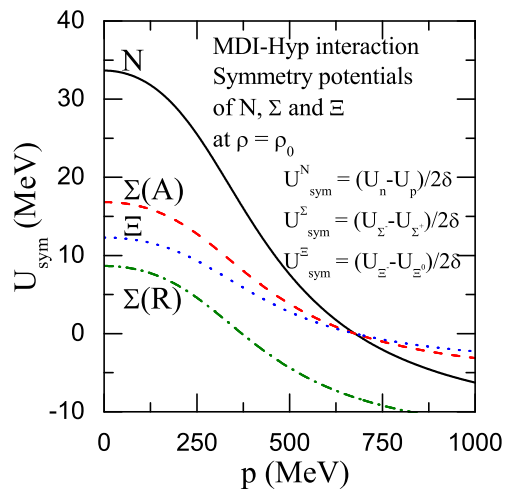


Fig. 14. (Color online) Momentum dependence of the symmetry potentials of nucleon, Σ and Ξ in asymmetric nuclear matter at saturation density $\rho = \rho_0$ with the MDI-Hyp-A and MDI-Hyp-R interactions. Taken from Ref. [199].

ter can thus be approximated as

$$U_{\tau_b}(\rho, p, \delta) \approx U_{\tau_b}(\rho, p, \delta = 0) - \tau_b U_{\text{sym}}^b(\rho, p)\delta, \quad (67)$$

where the symmetry potential $U_{\text{sym}}^b(\rho, p)$ can be obtained approximately by

$$U_{\text{sym}}^N(\rho, p) \approx (U_n(\rho, p, \delta) - U_p(\rho, p, \delta))/2\delta, \quad (68)$$

$$U_{\text{sym}}^\Sigma(\rho, p) \approx (U_{\Sigma^-}(\rho, p, \delta) - U_{\Sigma^+}(\rho, p, \delta))/2\delta, \quad (69)$$

$$U_{\text{sym}}^\Xi(\rho, p) \approx (U_{\Xi^-}(\rho, p, \delta) - U_{\Xi^0}(\rho, p, \delta))/2\delta, \quad (70)$$

for the nucleon as well as Σ and Ξ hyperons, respectively. Fig. 14 shows the momentum dependence of the symmetry potentials for nucleon, Σ and Ξ at saturation density ρ_0 with the MDI-Hyp-A and MDI-Hyp-R interactions, and these results are obtained from the single-particle potentials of nucleons as well as Σ and Ξ hyperons in asymmetric nuclear matter at ρ_0 and isospin asymmetry $\delta = 0.2$. One can see that all symmetry potentials at ρ_0 display strong momentum dependence and decrease with increasing momentum.

Although the symmetry potentials at saturation density ρ_0 are independent of the x parameter by construction in the MDI interaction as mentioned earlier, this is not the case at other densities. Shown in Fig. 15 are the momentum dependence of the symmetry potentials of the nucleon as well as the Σ and Ξ hyperons in asymmetric nuclear matter at density $\rho = 3\rho_0$ in the MDI-Hyp-A and MDI-Hyp-R interactions with $x = 0$ and $x = -1$. It is seen that the symmetry potentials depends strongly on the particle momentum and the x value used. For the Σ hyperon, its symmetry potential further depends on the choice of the MDI-Hyp-A interaction or the MDI-Hyp-R interaction. It should be mentioned that the charged Σ baryon ratio in heavy ion collisions has been proposed to constrain the symmetry energy (potential) at densities larger

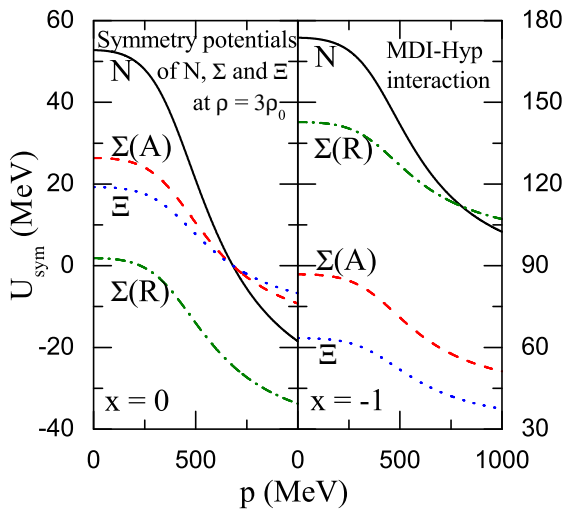


Fig. 15. (Color online) Same as Fig. 14 but at a density of $\rho = 3\rho_0$ and with $x = 0$ (left panel) and $x = -1$ (right panel). Taken from Ref. [199].

than $3\rho_0$ [224]. Therefore, it will be very interesting to see how the symmetry potentials of Σ and Ξ hyperons affect the charged Σ hyperon ratio and the charged Ξ hyperon ratio in intermediate and high energy heavy ion collisions induced by neutron-rich nuclei. This may be important for accurately constraining the high-density behavior of the symmetry energy using these ratios in heavy ion collisions. Therefore, the extended MDI interaction with hyperons is useful for studying the nuclear symmetry energy (potential) at high densities as well as the in-medium NN, NY, and YY effective interactions at extreme conditions of high baryon densities, high momentum, and high isospin, in transport model simulations for heavy ion collisions.

5.1.3 Hybrid stars

Besides heavy ion collisions in terrestrial laboratory, the compact objects (e.g., neutron stars) provide another important site in nature to test the in-medium effective interactions at high densities. Hyperons may appear in the interior of neutron stars. At higher densities in the core of a neutron star, a transition from the hadron matter to the quark matter is also expected to occur. This leads to the so-called hybrid star that is expected to have a hadron phase at low densities, a mixed phase of hadrons and quarks at moderate densities, and a quark core at high densities. The extended MDI interaction is thus useful for exploring the properties of the hybrid star. In the following, we review the results of the properties of hybrid stars with the extended MDI interaction.

For the hadron-quark phase transition, the Gibbs construction [225,226] is adopted with the quark phase described by a simple MIT bag model [227,228]. For the hadron interactions, only the MDI-Hyp-R interaction is used in the following since the repulsive ΣN interaction is

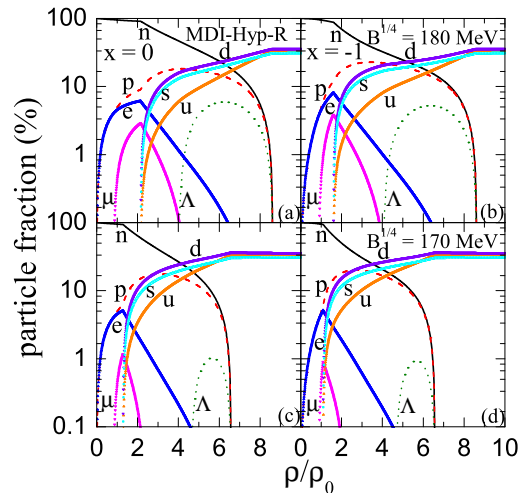


Fig. 16. (Color online) Particle fractions as functions of baryon density in a hypernuclear matter with the presence of a hadron-quark phase transition from the MDI-Hyp-R interaction with $x = 0$ ((a) and (c)) and $x = -1$ ((b) and (d)) for the hadron phase and the MIT bag model for the quark phase. Results from $B^{1/4} = 180$ MeV ((a) and (b)) and 170 MeV ((c) and (d)) are shown for comparison. Taken from Ref. [199].

more consistent with the latest empirical information [212, 213, 214, 215, 216]. Shown in Fig. 16 is baryon density dependence of the particle fractions of each species in the presence of a hadron-quark phase transition, with the hadron phase described by the MDI-Hyp-R interaction with $x = 0$ and $x = -1$ and the quark phase described by the MIT bag model with bag constants $B^{1/4} = 180$ MeV and 170 MeV. It is seen that the hadron-quark phase transition occurs at lower baryon density for a stiffer symmetry energy and for a smaller B value, while the density at the end of the hadron-quark phase transition essentially depend only on the B value but not much on the value of the x parameter. With a smaller B value, the hadron-quark phase transition both begins and ends at lower densities. In addition, one can see that only Λ hyperons (no other hyperons) appear in (and only in) the mixed phase in the present model. However, the fraction of Λ hyperons is sensitive to the B value with a smaller B value giving smaller fraction. Moreover, it should be mentioned that the fraction of hyperons is also sensitive to the NY and YY interactions [199]. In particular, as shown in Fig. 6 of Ref. [199], the Λ hyperon appears in hypernuclear matter at a baryon density of about 0.5 fm^{-3} with the extended MDI interaction. For the Σ hyperon, the critical density at which it appears in the hypernuclear matter depends strongly on the sign of the ΣN interaction. For the attractive MDI-Hyp-A interaction, the critical density for the appearance of Σ^- is about 0.3 fm^{-3} , whereas for the repulsive MDI-Hyp-R interaction, it does not appear until very high densities. These values are in good agreement with the values of about 0.6 for the Λ hyperon and 0.3 fm^{-3} for the Σ^- hyperon obtained from both the BHF+TBF [229] and the DBHF [230] with free non-interacting hyperons.

For a static hybrid star, it contains three parts from the center to the surface: the liquid core, the inner crust, and the outer crust. The liquid core is assumed to be the hypernuclear matter or that with the hadron-quark phase transition. For the inner crust, a parameterized EOS of $P = a + b\epsilon^{4/3}$ is adopted as in the previous treatment [47, 48]. The well-known BPS EOS [185] is used for the outer crust which consists of heavy nuclei and the electron gas. The transition density ρ_t between the liquid core and the inner crust is consistently determined as described earlier (see also Refs. [47, 48]), and for the density at the edge of inner crust and outer crust, it is taken to be $\rho_{\text{out}} = 2.46 \times 10^{-4} \text{ fm}^{-3}$. The parameters a and b are determined by the pressures (P) and energy densities (ϵ) at ρ_t and ρ_{out} . Using these EOS's, one can then calculate the mass-radius relation of hybrid stars with the well-known Tolman-Oppenheimer-Volkoff (TOV) equation.

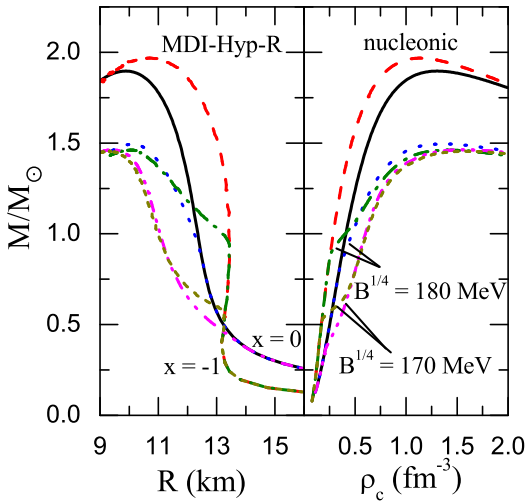


Fig. 17. (Color online) The hybrid star mass as a function of radius (left panel) and central density (right panel) using the MDI-Hyp-R interaction $x = 0$ and $x = -1$ for the hadron phase and MIT bag constant $B^{1/4} = 180$ and 170 MeV for the quark phase. Results from a pure nucleonic approach are also included for comparison. Taken from Ref. [199].

Displayed in Fig. 17 are the M-R and M- ρ_c relations for hybrid stars using the MDI-Hyp-R interaction with $x = 0$ and $x = -1$ for the hadron phase and $B^{1/4} = 180$ and 170 MeV for the quark phase. For comparison, the results from a pure nucleonic approach are also included. It is clearly seen that including the hadron-quark phase transition in neutron stars significantly reduces the maximum mass of neutron stars. For $B^{1/4} = 180$ MeV, the maximum mass is $1.50M_\odot$ for $x = 0$ and $1.46M_\odot$ for $x = -1$, while for $B^{1/4} = 170$ MeV it is $1.46M_\odot$ for $x = 0$ and $1.45M_\odot$ for $x = -1$, respectively. The radius of a standard neutron star with a mass of $1.4M_\odot$ is 11.0 km for $x = 0$ and

10.8 km for $x = -1$ if $B^{1/4} = 180$ MeV is used, while it becomes 10.2 km for $x = 0$ and 10.0 km for $x = -1$ if $B^{1/4} = 170$ MeV is used. If the B value is further reduced, the hadron-quark phase transition would happen at even lower densities, resulting in a smaller radius for the hybrid star. These features indicate that the radius of a neutron star with canonical mass $1.4M_\odot$ is not only sensitive to the stiffness of the symmetry energy, but to the hadron-quark phase transition.

Finally, we would like to point out that the original MDI interaction does not cause causality violation in β -stable $npe\mu$ matter at least up to baryon density of $10\rho_0$ as shown in Fig. 2(d) of Ref. [48]. Since the appearance of new degrees of freedom such as hyperons and quarks usually softens the EOS of neutron star matter, the causality condition is still satisfied for the extended MDI interaction, and this is verified by explicit calculations [199]. We also note that the causality condition is satisfied for symmetric nuclear matter at least up to $10\rho_0$ for the MDI interaction.

5.2 An improved MDI interaction with separate density dependence for neutrons and protons

In the MDI interaction, as pointed out before, the terms with parameter B (and σ) in Eqs. (16) and (17) can be obtained directly from the density-dependent two-body effective interaction Eq. (19), which represents an effective in-medium many-body force and has been extensively adopted in the Skyrme or Gogny interaction. Since the pp, nn, and np interactions in Eq. (19) all depend on the same total density $\rho = \rho_n + \rho_p$, the proper isospin dependence of the in-medium effective many-body forces is thus neglected. As pointed out earlier in Refs. [231, 232, 233, 234, 235, 236, 237], there is no *a priori* physical justification for such a density dependence in these interactions. On the other hand, within the Brueckner theory, it has been found that the G-matrix of NN interactions in isospin asymmetric nuclear matter depends strongly on the respective Fermi momenta of neutrons and protons (k_n and k_p) [238, 239]. It is thus physically more reasonable to assume that the interaction between neutrons depends on the neutron density, and that between protons on the proton density, instead of the total density ρ [231].

Indeed, the separate density dependence for pp, nn and np interactions has already been used in various models to better understand the structure of nuclei far from the β -stable line. For example, in the early 1960s and 1970s, local effective interactions with density dependence separately introduced for pp, nn, and np pairs were proposed by Sprung and Banerjee [240], Brueckner and Dabrowski [238, 239], and Negele [241]. Recently, Xu and Li [71] explored the effects of separate density dependence of neutrons and protons by replacing the density-dependent term in Eq. (19) with the following expression:

$$V_D = \frac{1}{6}t_3(1 + x_3P_\sigma)[\rho_{\tau_i}(\mathbf{r}_i) + \rho_{\tau_j}(\mathbf{r}_j)]^\gamma\delta(\mathbf{r}_{ij}), \quad (71)$$

where $\rho_\tau(\mathbf{r})$ denotes the density of nucleon τ (1 for neutrons and -1 for protons) at the coordinate \mathbf{r} . This density-dependent interaction changes the expressions for the terms with parameter B in the original MDI interaction. In particular, the B -term in Eq. (16) for the energy density, i.e.,

$$V_B = \frac{B}{\sigma + 1} \frac{\rho^{\sigma+1}}{\rho_0^\sigma} (1 - x\delta^2) \quad (72)$$

becomes

$$V'_B = \frac{B}{\sigma + 1} \frac{\rho^{\sigma+1}}{\rho_0^\sigma} \left\{ \frac{1+x}{2} (1 - \delta^2) + \frac{1-x}{4} [(1+\delta)^{\sigma+1} + (1-\delta)^{\sigma+1}] \right\}, \quad (73)$$

and the B -term in Eq. (17) for the single-particle potential, i.e.,

$$U_B = B \left(\frac{\rho}{\rho_0} \right)^\sigma (1 - x\delta^2) - 4\tau x \frac{B}{\sigma + 1} \frac{\rho^{\sigma-1}}{\rho_0^\sigma} \delta \rho_{-\tau} \quad (74)$$

becomes

$$U'_B = \frac{B}{2} \left(\frac{2\rho_\tau}{\rho_0} \right)^\sigma (1 - x) + \frac{2B}{\sigma + 1} \left(\frac{\rho}{\rho_0} \right)^\sigma \times (1 + x) \frac{\rho_{-\tau}}{\rho} \left[1 + (\sigma - 1) \frac{\rho_\tau}{\rho} \right]. \quad (75)$$

Similarly, the B -term in Eq. (35) for the symmetry energy, i.e.,

$$E_{\text{sym},B} = -\frac{Bx}{\sigma + 1} \left(\frac{\rho}{\rho_0} \right)^\sigma \quad (76)$$

changes to

$$E'_{\text{sym},B} = \frac{B}{\sigma + 1} \left(\frac{\rho}{\rho_0} \right)^\sigma \left[\frac{1-x}{4} \sigma(\sigma + 1) - \frac{1+x}{2} \right], \quad (77)$$

while the B -term in Eq. (38) for the symmetry potential, i.e.,

$$U_{\text{sym},B} = -2x \frac{B}{\sigma + 1} \left(\frac{\rho}{\rho_0} \right)^\sigma \quad (78)$$

changes to

$$U'_{\text{sym},B} = \frac{B}{\sigma + 1} \left(\frac{\rho}{\rho_0} \right)^\sigma \left[\frac{1-x}{2} \sigma(\sigma + 1) - 1 - x \right] \quad (79)$$

The x -dependent parameters $A_u(x)$ and $A_l(x)$ then become, respectively,

$$A'_u(x) = A_{u0} + \frac{2B}{\sigma + 1} \left[\frac{1-x}{4} \sigma(\sigma + 1) - \frac{1+x}{2} \right], \quad (80)$$

and

$$A'_l(x) = A_{l0} - \frac{2B}{\sigma + 1} \left[\frac{1-x}{4} \sigma(\sigma + 1) - \frac{1+x}{2} \right]. \quad (81)$$

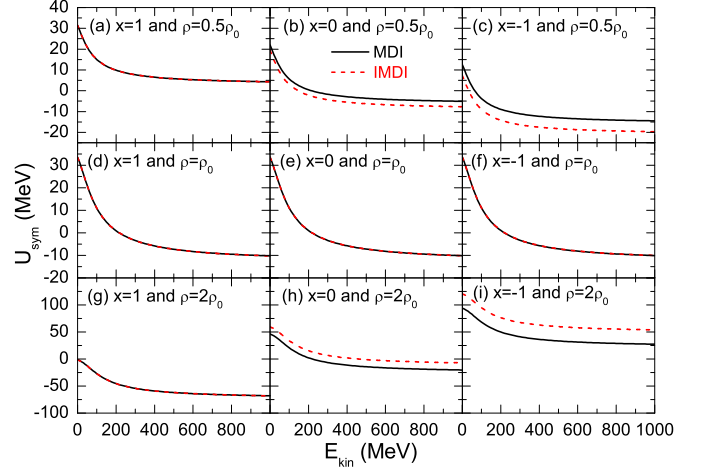


Fig. 18. The nuclear symmetry potential as a function of the nucleon kinetic energy from both the MDI interaction (solid lines) and the IMDI interaction (dashed lines) at density of $\rho = \rho_0/2, \rho_0,$ and $2\rho_0$.

It should be noted that the expressions in Eqs. (77), (80), and (81) are different from the corresponding ones in Ref. [71] where the parabolic approximation Eq. (3) has been used to calculate the symmetry energy while here the symmetry energy is obtained from the definition of Eq. (2).

To illustrate the effects of the separate density dependence for neutrons and protons, we show in Fig. 18 the kinetic energy dependence of the symmetry potential at density $\rho = \rho_0/2, \rho_0,$ and $2\rho_0$, using the improved MDI (IMDI) interaction. The results from the MDI interaction are also included for comparison. Three typical values of the x parameter, i.e., $x = 1, 0,$ and -1 are used. It is seen from panels (a), (d), and (g) that the symmetry potentials from the MDI and IMDI are exactly the same for $x = 1$ due to the fact that Eq. (79) is reduced to Eq. (78) for $x = 1$. Furthermore, one can see from panels (d), (e), and (f) that the symmetry potentials from the MDI and IMDI interactions are also exactly the same at $\rho = \rho_0$ for different x values due to construction (See, e.g., Eqs. (80) and (81)). For the cases with $x = 0$ and -1 , one can see from panels (b), (c), (h), and (i) that the symmetry potential from the IMDI interaction deviates significantly from the one from the MDI interaction at $\rho \neq \rho_0$. Therefore, one can expect that the symmetry energy from the MDI and IMDI interactions for both $x = 0$ and -1 will give significantly different density behaviors for the symmetry energy, and this indeed can be seen from Fig. 19 where the density dependence of the symmetry energies from the MDI and IMDI interactions are compared. For $x = 1$, as expected, one can see that the symmetry energy is the same for both the MDI and IMDI interactions since the $U_{\text{sym}}(\rho, p)$ remains unchanged for $x = 1$ (see Fig. 18). For $x = 0$ and -1 , however, one can see from Fig. 19 that the symmetry energy from the IMDI interaction becomes significantly stiffer compared to that from the MDI interaction. These features are consistent with the variations

of the symmetry potential $U_{\text{sym}}(\rho, p)$ obtained from the MDI and IMDI interactions as shown in Fig. 18.

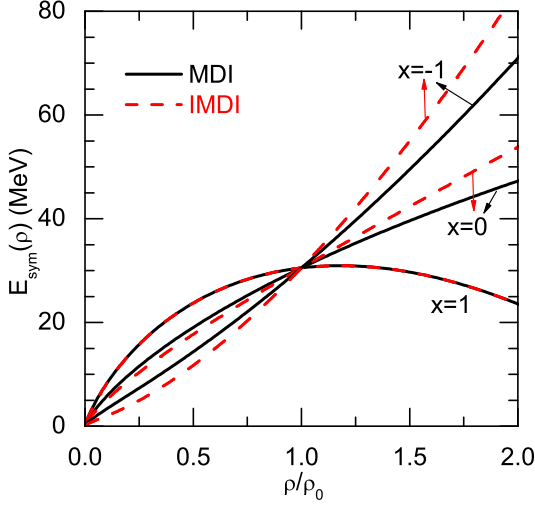


Fig. 19. Density dependence of the symmetry energy in the MDI interaction (solid lines) and the IMDI interaction (dashed lines) with $x = 1, 0$, and -1 .

6 Summary and outlook

We have reviewed the isospin- and momentum-dependent MDI interaction that has been developed during recent years. The MDI interaction has been systematically and successfully applied in the study of the transport model simulations of heavy ion collisions induced by neutron-rich nuclei, the thermal properties of asymmetric nuclear matter including the liquid-gas phase transition, and the properties of neutron stars. Through comparing with the available experimental data, these studies based on the MDI interaction provide, via a phenomenological way, important information and understanding on the in-medium nuclear effective interaction, especially its isospin and momentum dependence. And this further puts important constraints on the EOS of asymmetric nuclear matter, especially the density dependence of the symmetry energy.

We have emphasized the importance of the momentum dependence of the nuclear mean-field potential in nuclear medium, including its isovector symmetry potential. The IBUU04 transport model simulations of heavy ion collisions with the MDI interaction indicate that the momentum dependence of the nucleon isoscalar potential and isovector symmetry potential plays an important role in the degree of isospin diffusion and the energy dependence of $t/{}^3\text{He}$ ratio in heavy ion collisions. In fact, the IBUU04 transport model analysis on the isospin diffusion data from NSCL-MSU has already put important constraints on the density dependence of the symmetry energy. The momentum dependence of the nucleon isoscalar potential and isovector symmetry potential also plays an important role in understanding the thermal properties of

asymmetric nuclear matter. This has been demonstrated from the studies on the temperature dependence of the symmetry energy and symmetry free energy, liquid-gas phase transition of asymmetric nuclear matter, and especially the novel differential isospin fractionation phenomenon in asymmetric nuclear matter. Moreover, the isospin- and momentum-dependent MDI interaction has been successfully used to explore the core-crust transition of neutron stars, and important constraints on the transition density and pressure at the inner edge of neutron stars have been obtained through using the MDI interaction parameters constrained by terrestrial laboratory data.

Furthermore, we have introduced two extensions of the MDI interaction that have been made recently. One is the extended MDI interaction for the baryon octet and the other is the improved MDI interaction with separate density dependence for neutrons and protons. The latter takes into account more accurately the isospin dependence of the in-medium many-body interactions and thus may provide a more physically reasonable density functional for the isospin dependence of the in-medium nuclear effective interaction. As for the extended MDI interaction for the baryon octet, we would like to emphasize that it is useful not only in understanding the properties of hybrid stars as discussed in the present paper, but also in investigating strangeness production and its isospin effects in heavy ion collisions induced by neutron-rich nuclei at higher energies (a few GeV/nucleon), and thus is potentially important for exploring the high density behaviors of the symmetry energy and the in-medium effective interactions between nucleon-hyperon and hyperon-hyperon.

Although the MDI interaction has been used for different studies as described in this paper, it still can be improved in some aspects. For example, the MDI interaction predicts an attractive isoscalar single-particle potential at high momenta/energies in symmetric nuclear matter at saturation density, which is significantly weaker than the empirical optical potential (see, e.g., Fig. 13) when the nucleon momentum is larger than about 550 MeV/c (i.e., the nucleon kinetic energy of about 160 MeV). This is due to the fact that the parameters of the MDI interaction are obtained from fitting the single-particle potential from the Gogny-D1 interaction that fails to describe the high-momentum/energy behaviors of the empirical optical model potential, although it can give a good description of the properties of finite nuclei. Therefore, it will be interesting to re-fit the values of the parameters in the MDI interaction to obtain a reasonable high energy behaviors for the isoscalar single-particle potential and study its effects in transport model simulations of heavy ion collisions at higher incident energies (larger than about 200 MeV/nucleon). In addition, the MDI interaction has been mainly used so far to explore the isospin-dependent properties of nuclear matter, and it will be very interesting to see how the MDI interaction describe the spin-dependent properties of asymmetric nuclear matter, especially the density and asymmetry at which the ferromagnetic transition can occur in an asymmetric nuclear matter. These works are in progress and will be reported elsewhere.

Finally, we would like to point out that the high baryon density and/or large isospin asymmetry reached in heavy ion collisions induced by neutron-rich nuclei provide a unique experimental condition to probe the isospin- and momentum-dependent effective interaction in high density asymmetric nuclear matter. Indeed, this has already been demonstrated from studying the isospin effects in heavy ion collisions induced by neutron-rich nuclei based on the transport model simulations with the MDI interaction. In addition, the high baryon density and large isospin asymmetry expected in the interior of neutron stars provide another excellent astrophysical condition to probe the isospin- and momentum-dependent effective interaction in high density asymmetric nuclear matter, and this has been demonstrated from studying the properties of hybrid stars with the extended MDI interaction for the baryon octet.

Acknowledgments

This work was supported by the National Natural Science Foundation of China under Grant No. 11275125, 11135011, 11175085, 11235001, and 11035001, the Shanghai Rising-Star Program under Grant No. 11QH1401100, the “Shu Guang” project supported by Shanghai Municipal Education Commission and Shanghai Education Development Foundation, the Program for Professor of Special Appointment (Eastern Scholar) at Shanghai Institutions of Higher Learning, the Science and Technology Commission of Shanghai Municipality (11DZ2260700), the Project Funded by the Priority Academic Program Development of Jiangsu Higher Education Institutions (PAPD), the “100-talent plan” of Shanghai Institute of Applied Physics under grant Y290061011 from the Chinese Academy of Sciences, the US National Science Foundation under Grant No. PHY-1068572 and PHY-1068022, the Welch Foundation under Grant No. A-1358, the US National Aeronautics and Space Administration under grant NNX11AC41G issued through the Science Mission Directorate, and the CUSTIPEN (China-U.S. Theory Institute for Physics with Exotic Nuclei) under DOE grant number DE-FG02-13ER42025.

References

1. B.A. Li, C.M. Ko, and W. Bauer, topical review, *Int. Jour. Mod. Phys. E* **7**, (1998) 147.
2. *Isospin Physics in Heavy-Ion Collisions at Intermediate Energies*, Eds. Bao-An Li and W. Udo Schröder (Nova Science Publishers, Inc, New York, 2001).
3. J.M. Lattimer and M. Prakash, *Phys. Rep.* **333**, 121 (2000); *Science* **304**, (2004) 536.
4. P. Danielewicz, R. Lacey, and W.G. Lynch, *Science* **298**, (2002) 1592.
5. V. Baran, M. Colonna, V. Greco, and M. Di Toro, *Phys. Rep.* **410**, (2005) 335.
6. A.W. Steiner, M. Prakash, J.M. Lattimer, and P.J. Ellis, *Phys. Rep.* **411**, (2005) 325.
7. L.W. Chen, C.M. Ko, B.A. Li, and G.C. Yong, *Front. Phys. China* **2**, (2007) 327 [arXiv:0704.2340].
8. B.A. Li, L.W. Chen, and C.M. Ko, *Phys. Rep.* **464**, (2008) 113.
9. K.A. Brueckner, S.A. Coon and J. Dabrowski, *Phys. Rev.* **168**, (1967) 1184.
10. P.J. Siemens, *Nucl. Phys.* **A141**, (1970) 225.
11. O. Sjöberg, *Nucl. Phys.* **A222**, (1974) 161.
12. I. Bombaci and U. Lombardo, *Phys. Rev. C* **44**, (1991) 1892.
13. W. Zuo, A. Lejeune, U. Lombardo, J. F. Mathiot, *Eur. Phys. J. A* **14**, (2002) 469.
14. B. ter Haar and R. Malfliet, *Phys. Rep.* **149**, (1987) 207.
15. H. Mütter and A. Polls, *Prog. Part. Nucl. Phys.* **45**, (2000) 243.
16. W.H. Dickhoff and C. Barbieri, *Prog. Part. Nucl. Phys.* **52**, (2004) 377.
17. B. Friedman and V.R. Pandharipande, *Nucl. Phys.* **A361**, (1981) 502.
18. I.E. Lagaris and V.R. Pandharipande, *Nucl. Phys.* **A369**, (1981) 470.
19. A. Akmal, V. R. Pandharipande, and D. G. Ravenhall, *Phys. Rev. C* **58**, (1998) 1804.
20. B.D. Serot and J.D. Walecka, *Int. Jour. Mod. Phys. E* **6**, (1997) 515.
21. R.J. Furnstahl, *Lect. Notes Phys.* **641**, (2004) 1.
22. D. Vretenar and W. Weise, *Lect. Notes Phys.* **641**, (2004) 65.
23. B.D. Serot and J.D. Walecka, *Adv. Nucl. Phys.* **16**, (1986) 1.
24. S.A. Chin, *Ann. Phys. (N.Y.)*, **108**, (1977) 301.
25. P.-G. Reinhard, *Rep. Prog. Phys.* **52**, (1989) 439.
26. P. Ring, *Prog. Part. Nucl. Phys.* **37**, (1996) 193.
27. D. Vautherin and D. M. Brink, *Phys. Rev. C* **5**, (1972) 626.
28. M. Brack, C. Guet and H. -B. Hakansson, *Phys. Rep.* **123**, (1985) 275.
29. J.R. Stone and P.-G. Reinhard, *Prog. Part. Nucl. Phys.* **58**, (2007) 587.
30. J. Treiner *et al.*, *Ann. Phys. (N.Y.)*, **170**, (1986) 406.
31. D. Bandyopadhyay, C. Samanta, S.K. Samaddar and J.N. De, *Nucl. Phys.* **A511**, (1990) 1.
32. D.N. Basu, *Phys. Lett.* **B566**, (2003) 90.
33. D.N. Basu, P.R. Chowdhury, C. Samanta, *Phys. Rev. C* **72**, (2005) 051601(R).
34. T. Mukhopadhyay and D. N. Basu, *Nucl. Phys.* **A789**, (2007) 201.
35. D.N. Basu, P. Roy Chowdhury, and C. Samanta, *Nucl. Phys.* **A811**, (2008) 140.
36. D.N. Basu, P. Roy Chowdhury, and C. Samanta, *Phys. Rev. C* **80**, (2009) 057304.
37. P. Roy Chowdhury, D.N. Basu, and C. Samanta, *Phys. Rev. C* **80**, (2009) 011305(R).
38. T.R. Routray, S.K. Tripathy, B.B. Dash, B. Behera, and D.N. Basu, *Eur. Phys. J. A* **47**, (2011) 92.
39. T.R. Routray, X. Vinas, S.K. Tripathy, M. Bhuyan, S.K. Patra, and B. Behera, arXiv:1208.4236.
40. T. Gaitanos and M. Kaskulov, *Nucl. Phys.* **A899**, (2013) 133.
41. D.N. Basu, arXiv:1309.6793, 2013.
42. A.E.L. Dieperink, Y. Dewulf, D. Van Neck, M. Waroquier, and V. Rodin, *Phys. Rev. C* **68**, (2003) 064307.
43. Z.H. Li, U. Lombardo, H.-J. Schulze, W. Zuo, L.W. Chen, and H.R. Ma, *Phys. Rev. C* **74**, (2006) 047304.
44. B.J. Cai and L.W. Chen, *Phys. Rev. C* **85**, (2012) 024302.

45. F.S. Zhang and L.W. Chen, *Chin. Phys. Lett.* **18**, (2001) 142.
46. A.W. Steiner, *Phys. Rev. C* **74**, (2006) 045808.
47. J. Xu, L.W. Chen, B.A. Li, and H.R. Ma, *Phys. Rev. C* **79**, (2009) 035802.
48. J. Xu, L.W. Chen, B.A. Li, and H.R. Ma, *Astrophys. J.* **697**, (2009) 1549.
49. L.W. Chen, *Science China: Physics, Mechanics and Astronomy* **54**, (2011) s124 [arXiv:1101.2384].
50. Z. Zhang and L.W. Chen, *Phys. Lett.* **B726**, (2013) 234.
51. C. Xu, B. A. Li, L. W. Chen, and C. M. Ko, *Nucl. Phys. A* **865**, (2011) 1.
52. R. Chen, B.J. Cai, L.W. Chen, B.A. Li, X.H. Li, and C. Xu, *Phys. Rev. C* **85**, (2012) 024305.
53. A. M. Lane, *Nucl. Phys.* **35**, (1962) 676.
54. B.A. Li, *Phys. Rev. C* **69**, (2004) 034614.
55. C. Xu, B. A. Li, and L. W. Chen, *Phys. Rev. C* **82**, (2010) 054607.
56. B.J. Cai and L.W. Chen, *Phys. Lett.* **B711**, (2012) 104.
57. X. H. Li, B. J. Cai, L. W. Chen, R. Chen, B. A. Li, and C. Xu, *Phys. Lett.* **B 721**, (2013) 101.
58. C. Xu, B.A. Li, and L.W. Chen, contribution in this volume [arXiv:1308.1502].
59. G.F. Bertsch and S. Das Gupta, *Phys. Rep.* **160**, (1988) 189.
60. B. Behera and R.K. Satpathy, *J. Phys. G* **5**, (1979) 85.
61. J. Decharge and D. Gogny, *Phys. Rev. C* **21** (1980) 1568.
62. R. Wiringa, *Phys. Rev. C* **38**, (1988) 2967.
63. L.P. Csernai, G. Fai, C. Gale, and E. Osnes, *Phys. Rev. C* **46**, (1992) 736.
64. B. Behera, T.R. Routray, and R.K. Satpathy, *J. Phys. G* **23**, (1997) 445.
65. B. Behera, T.R. Routray, and R.K. Satpathy, *J. Phys. G* **24**, (1998) 2073.
66. C. Gale, G. Bertsch, and S. Das Gupta, *Phys. Rev. C* **35**, (1987) 1666.
67. G.M. Welke, M. Prakash, T. T. S. Kuo, S. Das Gupta, and C. Gale, *Phys. Rev. C* **38**, (1988) 2101.
68. I. Bombaci, in Ref. [2], p.35.
69. C.B. Das, S. Das Gupta, C. Gale, and B.A. Li, *Phys. Rev. C* **67**, (2003) 034611.
70. L.W. Chen, C.M. Ko, and B.A. Li, *Phys. Rev. Lett.* **94**, (2005) 032701.
71. C. Xu and B.A. Li, *Phys. Rev. C* **81**, (2010) 044603.
72. J.R. Stone, J.C. Miller, R. Konciewicz, P.D. Stevenson, M.R. Strayer, *Phys. Rev. C* **68**, (2003) 034324.
73. C. Xu and B.A. Li, *Phys. Rev. C* **81**, (2010) 064612.
74. J. Xu and C.M. Ko, *Phys. Rev. C* **82**, (2010) 044311.
75. B. Behera, T.R. Routray, B. Sahoo, and R.K. Satpathy, *Nucl. Phys.* **A699**, (2002) 770.
76. B. Behera, T.R. Routray, A. Pradhan, S.K. Patra, and P.K. Sahu, *Nucl. Phys.* **A753**, (2005) 367.
77. B. Behera, T.R. Routray, A. Pradhan, S.K. Patra, and P.K. Sahu, *Nucl. Phys.* **A794**, (2007) 132.
78. B. Behera, T.R. Routray, and S K Tripathy, *J. Phys. G* **38**, (2011) 115104.
79. B.A. Li, C. B. Das, S. Das Gupta, and C. Gale, *Phys. Rev. C* **69**, (2004) 011603(R); *Nucl. Phys.* **A735**, (2004) 563.
80. L.W. Chen, C.M. Ko, and B.A. Li, *Phys. Rev. C* **69**, (2004) 054606.
81. B.A. Li, G.C. Yong and W. Zuo, *Phys. Rev. C* **71**, (2005) 014608.
82. B.A. Li, G.C. Yong and W. Zuo, *Phys. Rev. C* **71**, (2005) 044604.
83. B.A. Li and L.W. Chen, *Phys. Rev. C* **72**, (2005) 064611.
84. B.A. Li, L.W. Chen, G.C. Yong, and W. Zuo, *Phys. Lett.* **B634**, (2006) 378.
85. G.C. Yong, B.A. Li, L.W. Chen, and W. Zuo, *Phys. Rev. C* **73**, (2006) 034603.
86. G.C. Yong, B.A. Li, L.W. Chen, *Phys. Rev. C* **74**, (2006) 064617.
87. G.C. Yong, B.A. Li, and L.W. Chen, *Phys. Lett.* **B650**, (2007) 344.
88. J. Xu, L.W. Chen, B.A. Li and H.R. Ma, *Phys. Rev. C* **75**, (2007) 014607.
89. J. Xu, L.W. Chen, B.A. Li and H.R. Ma, *Phys. Lett.* **B650**, (2007) 348.
90. J. Xu, L.W. Chen, B.A. Li and H.R. Ma, *Phys. Rev. C* **77**, (2008) 014302.
91. L.W. Chen, C.M. Ko, and B.A. Li, *Phys. Rev. C* **76**, 054316 (2007).
92. W. Zuo, U. Lombardo, H.-J. Schulze, and Z.H. Li, *Phys. Rev. C* **74**, (2006) 014317.
93. E.N.E. van Dalen, C. Fuchs, and A. Faessler, *Phys. Rev. C* **72**, (2005) 065803.
94. L.W. Chen, C.M. Ko, and B.A. Li, *Phys. Rev. C* **72**, (2005) 064606.
95. Z.H. Li, L.W. Chen, C.M. Ko, B.A. Li, and H.R. Ma, *Phys. Rev. C* **74**, (2006) 044613.
96. D.P. Murdock and C.J. Horowitz, *Phys. Rev. C* **35**, (1987) 1442.
97. J.A. McNeil, L. Ray, and S.J. Wallace, *Phys. Rev. C* **27**, (1983) 2123.
98. M. Jaminon and C. Mahaux, *Phys. Rev. C* **40**, (1989) 354.
99. J.W. Negele and H. Orland, *Quantum Many-Particle System*, Perseus Books Publishing, L.L.C., 1998.
100. E.N.E. van Dalen, C. Fuchs and A. Faessler, *Nucl. Phys.* **A741**, (2004) 227; *Phys. Rev. Lett.* **95**, (2005) 022302.
101. O. Sjöberg, *Nucl. Phys.* **A265**, (1976) 511.
102. Z.Y. Ma, J. Rong, B.Q. Chen, Z.Y. Zhu and H.Q. Song, *Phys. Lett.* **B604**, (2004) 170.
103. W. Zuo, L.G. Gao, B.A. Li, U. Lombardo and C.W. Shen, *Phys. Rev. C* **72**, (2005) 014005.
104. F. Sammarruca, W. Barredo and P. Krastev, *Phys. Rev. C* **71**, (2005) 064306.
105. X.H. Li and L.W. Chen, *Nucl. Phys. A* **874**, (2012) 62.
106. J.W. Negele and K. Yazaki, *Phys. Rev. Lett.* **62**, (1981) 71.
107. V.R. Pandharipande and S.C. Pieper, *Phys. Rev. C* **45**, (1991) 791.
108. G.Q. Li and R. Machleidt, *Phys. Rev. C* **48**, (1994) 1702; *ibid*, *C 49*, (1994) 566.
109. F. Sammarruca and P. Krastev, nucl-th/0506081, 2005.
110. G.F. Bertsch, G.E. Brown, V. Koch, and B.A. Li, *Nucl. Phys.* **A490**, (1988) 745.
111. G.J. Mao, Z.X. Li, Y.Z. Zhuo, Y.L. Han, and Z.Q. Yu, *Phys. Rev. C* **49**, (1994) 3137; G.G. Mao, Z.X. Li and Y.Z. Zhuo, *ibid*, *C 53*, (1996) 2933; *C 55*, (1997) 792.
112. T. Caitanos, C. Fuchs and H.H. Wolter, *Phys. Lett* **B609**, (2005) 241.
113. Z.G. Xiao, B.A. Li, L.W. Chen, G.C. Yong, and M. Zhang, *Phys. Rev. Lett.* **102**, (2009) 062502.
114. M. Zhang et al., *Phys. Rev. C* **80**, (2009) 034616.
115. M. Zhang et al., *Phys. Rev. C* **82**, (2010) 044602.

116. G.C. Yong, B.A. Li and L.W. Chen, Phys. Lett. **B661**, (2008) 82.
117. Z.G. Xiao, G.C. Yong, L.W. Chen, B.A. Li, G.Q. Xiao, and N. Xu, contribution in this volume [arXiv:1312.5790].
118. M.B. Tsang et al., Phys. Rev. Lett. **92**, (2004) 062701.
119. F. Rami et al., Phys. Rev. Lett. **84**, (2000) 1120.
120. G.F. Bertsch, H. Kruse and S. Das Gupta, Phys. Rev. C **29**, (1984) 673.
121. L. Shi and P. Danielewicz, Phys. Rev. C **68**, (2003) 064604.
122. B.A. Li, C.M. Ko, Z.Z. Ren, Phys. Rev. Lett. **78**, (1997) 1644.
123. L.W. Chen, C.M. Ko, B.A. Li, Phys. Rev. C **68**, (2003) 017601; Nucl. Phys. **A729**, (2003) 809.
124. P.E. Hodgson and E. Běták, Phys. Rep. **374**, (2003) 1; and the references therein.
125. L.P. Csernai and J.I. Kapusta, Phys. Rep. **131**, (1986) 223; and the references therein.
126. M. Gyulassy, K. Frankel, and E.A. Relmer, Nucl. Phys. **A402**, (1983) 596.
127. J. Aichelin, A. Rosenhauer, G. Peilert, H. Stöcker, and W. Greiner, Phys. Rev. Lett. **58**, (1987) 1926.
128. V. Koch *et al.*, Phys. Lett. **B241**, (1990) 174.
129. P. Pawłowski *et al.*, Eur. Phys. Jour. A **9**, (2000) 371.
130. R. Mattiello *et al.*, Phys. Rev. Lett. **74**, (1995) 2180; R. Mattiello *et al.*, Phys. Rev. C **55**, (1997) 1443.
131. J. L. Nagle *et al.*, Phys. Rev. C **53**, (1996) 367.
132. A. Polleri et al., Nucl. Phys. **A661**, (1999) 452c.
133. K. Hagel *et al.*, Phys. Rev. C **62**, (2000) 034607.
134. J. Cibor *et al.*, Phys. Lett. **B473**, (2000) 29.
135. L.G. Sobotka, R.J. Charity, and J.F. Dempsey, in Ref. [2], p.331.
136. M. Veselsky *et al.*, Phys. Lett. **B497**, (2001) 1.
137. Ph. Chomaz and F. Gulminelli, Phys. Lett. **B447**, (1999) 221.
138. L.W. Chen, F.S. Zhang, Z.H. Lu, W.F. Li, Z.Y. Zhu, and H.R. Ma, J. Phys. G **27**, (2001) 1799.
139. W. Zuo et al., Phys. Rev. C **69**, (2003) 064001; *ibid.* C **73**, (2006) 035208.
140. B.A. Li and L.W. Chen, Phys. Rev. C **74**, (2006) 034610.
141. Ch. C. Moustakidis, Phys. Rev. C **76**, (2007) 025805.
142. J.N. De and S.K. Samaddar, Phys. Rev. C **85**, (2012) 024310.
143. P. Donati, P.M. Pizzochero, P.F. Bortignon, and R.A. Broglia, Phys. Rev. Lett. **72**, (1994) 2835.
144. D.J. Dean, S.E. Koonin, K. Langanke, and P.B. Radha, Phys. Lett. **B356**, (1995) 429; D.J. Dean, K. Langanke, and J.M. Sampaio, Phys. Rev. C **66**, (2002) 045802.
145. C. Gale, G. M. Welke, M. Prakash, S. J. Lee, and S. Das Gupta, Phys. Rev. C **41**, (1990) 1545.
146. S.J. Lee and A.Z. Mekjian, Phys. Rev. C **63**, (2001) 044605.
147. A.Z. Mekjian, S.J. Lee, and L. Zamick, Phys. Rev. C **72**, (2005) 044305.
148. M.B. Tsang *et al.*, Phys. Rev. Lett. **86**, (2001) 5023.
149. D. V. Shetty et al., Phys. Rev. C **70**, (2004) 011601(R); D. V. Shetty et al., *ibid.* C **71**, (2005) 024602; D.V. Shetty et al., arXiv:nucl-ex/0603016.
150. G.A. Souliotis et al., Phys. Rev. C **73**, (2006) 024606; J. Iglío et al., *ibid.* C **74**, (2006) 024605; G. A. Souliotis et al., arXiv:nucl-ex/0603006.
151. D.V. Shetty et al., arXiv:nucl-ex/0606032.
152. A. Le Fèvre et al. for the ALADIN and INDRA collaborations, Phys. Rev. Lett. **94**, (2005) 162701.
153. W. Trautmann et al. for the ALADIN and INDRA collaborations, Proceedings of the IWM2005, Catania, Italy, Nov 2005 [arXiv:nucl-ex/0603027].
154. S. Kowalski et al., Phys. Rev. C **75**, (2007) 014601.
155. M.B. Tsang et al., Phys. Rev. C **64**, (2001) 054615.
156. A.S. Botvina, O.V. Lozhkin and W. Trautmann, Phys. Rev. C **65**, (2002) 044610.
157. A. Ono, P. Danielewicz, W.A. Friedman, W.G. Lynch and M.B. Tsang, Phys. Rev. C **68**, (2003) 051601(R); *ibid.* C **70**, (2004) 041604; arXiv:nucl-ex/0507018.
158. C.O. Dorso, C.R. Escudero, M. Ison, and J.A. López, Phys. Rev. C **73**, (2006) 044601.
159. Y.G. Ma et al., Phys. Rev. C **69**, (2004) 064610; Y.G. Ma et al., *ibid.* C **72**, (2005) 064603; W.D. Tian et al., Chin. Phys. Lett. **22**, (2005) 306.
160. C.J. Horowitz and A. Schwenk, Nucl. Phys. **A776**, (2006) 55.
161. J.B. Natowitz et al., Phys. Rev. Lett. **104**, (2010) 202501.
162. S. Typel, H.H. Wolter, G. Ropke, and D. Blaschke, contribution in this Volume [arXiv:1309.6934v1].
163. D. Q. Lamb, J. M. Lattimer, C. J. Pethick, and D. G. Ravenhall, Phys. Rev. Lett. **41**, (1978) 1623.
164. J.E. Finn et al., Phys. Rev. Lett. **49**, (1982) 1321.
165. G.F. Bertsch and P.J. Siemens, Phys. Lett. **B126**, (1983) 9.
166. H. Jaqaman, A. Z. Mekjian, and L. Zamick, Phys. Rev. C **27**, (1983) 2782; *ibid.* C **29**, (1984) 2067.
167. Ph. Chomaz, M. Colonna, and J. Randrup, Phys. Rep. **389**, (2004) 263.
168. C.B. Das, S. Das Gupta, W.G. Lynch, A.Z. Mekjian, and M.B. Tsang, Phys. Rep. **406**, (2005) 1.
169. *Dynamics and Thermodynamics with Nucleonic Degrees of Freedom*, Eds. Ph. Chomaz, F. Gulminelli, W. Trautmann and S.J. Yennello, Springer, (2006).
170. H. Müller and B.D. Serot, Phys. Rev. C **52**, (1995) 2072.
171. W.L. Qian, R.K. Su, and P. Wang, Phys. Lett. **B491**, (2000) 90.
172. H.S. Xu *et al.*, Phys. Rev. Lett. **85**, (2000) 716.
173. B.A. Li, L.W. Chen, H.R. Ma, J. Xu, and G.C. Yong, Phys. Rev. C **76**, (2007) 051601(R).
174. D.G. Ravenhall, C.J. Pethick, and J.R. Wilson, Phys. Rev. Lett. **50**, (1983) 2066.
175. K. Oyamatsu, Nucl. Phys. **A561**, (1993) 431.
176. C.J. Horowitz et al., Phys. Rev. C **69**, (2004) 045804; C.J. Horowitz et al., Phys. Rev. C **70**, (2004) 065806.
177. A.W. Steiner, Phys. Rev. C **77**, (2008) 035805.
178. C. J. Pethick, D. G. Ravenhall and C. P. Lorenz, Nucl. Phys. **A584**, (1995) 675.
179. F. Douchin and P. Haensel, Phys. Lett. **B485**, (2000) 107.
180. F. Douchin and P. Haensel, A&A **380**, (2001) 151.
181. J. Carriere, C.J. Horowitz, and J. Piekarewicz, Astrophys. J. **593**, (2003) 463.
182. S. Kubis, Phys. Rev. C **76**, (2007) 035801; Phys. Rev. C **70**, (2004) 065804.
183. J.M. Lattimer and M. Prakash, Phys. Rep. **442**, (2007) 109.
184. A. Worley, P.G. Krastev, and B.A. Li, Astrophys. J. **685**, (2008) 390.
185. G. Baym, C. Pethick, and P. Sutherland, Astrophys. J. **170**, (1971) 299.

186. G. Baym, H.A. Bethe, and C.J. Pethick, Nucl. Phys. **A175**, (1971) 225.
187. C.J. Pethick and D.G. Ravenhall, Ann. Rev. Nucl. Part. Sci. **45**, (1995) 429.
188. K. Oyamatsu and K. Iida, Phys. Rev. C **75**, (2007) 015801.
189. C. Ducoin, Ph. Chomaz, and F. Gulminelli, Nucl. Phys. **A789**, (2007) 403.
190. C. Providência, L. Brito, S.S. Avancini, D.P. Menezes, and P. Chomaz, Phys. Rev. C **73**, (2006) 025805.
191. C. Ducoin, J. Margueron, and P. Chomaz, Nucl. Phys. **A809**, (2008) 30.
192. C. Ducoin, C. Providência, A.M. Santos, L. Brito, and P. Chomaz, Phys. Rev. C **78**, (2008) 055801.
193. H. Pais, A. Santos, L. Brito, and C. Providência, Phys. Rev. C **82**, (2010) 025801.
194. C.J. Horowitz and J. Piekarewicz, Phys. Rev. Lett. **86**, (2001) 5647; Phys. Rev. C **64**, (2001) 062802(R); Phys. Rev. C **66**, (2002) 055803.
195. B. Link, R.I. Epstein, and J.M. Lattimer, Phys. Rev. Lett. **83**, (1999) 3362.
196. J. Arponen, Nucl. Phys. **A191**, (1972) 257.
197. L.W. Chen, Proceedings of the 14th National Conference on Nuclear Structure in China (NSC2012), Eds. J Meng, C.W. Shen, E.G. Zhao, S.G. Zhou (World Scientific, Singapore, 2012), pp. 43-54 [arXiv:1212.0284].
198. J.M. Lattimer, C.J. Pethick, M. Prakash, and P. Haensel, Phys. Rev. Lett. **66**, (1991) 2701.
199. J. Xu, L.W. Chen, C.M. Ko, and B.A. Li, Phys. Rev. C **81**, (2010) 055803.
200. O. Hashimoto and H. Tamura, Prog. Part. Nucl. Phys. **57**, (2006) 564.
201. C.B. Dover, D.J. Millener, and A. Gal, Phys. Rep. **184**, (1989) 1.
202. S. Bart, et al., Phys. Rev. Lett. **83**, (1999) 5238.
203. C.B. Dover and A. Gal, Ann. Phys. **146**, (1983) 309.
204. P.M.M. Maessen, Th. A. Rijken, and J.J. de Swart, Phys. Rev. C **40**, (1989) 2226.
205. A. Reuber, K. Holinda, and J. Speth, Nucl. Phys. **A570**, (1994) 543.
206. J. Dabrowski, Phys. Rev. C **60**, (1999) 025205.
207. D.J. Millener, C.B. Dover, and A. Gal, Phys. Rev. C **38**, (1988) 2700.
208. R.E. Chrien and C.B. Dover, Ann. Rev. Nucl. Part. Sci. **39**, (1989) 227.
209. S. Aoki, et al., Phys. Lett. **B355**, (1995) 45.
210. T. Fukuda, et al., Phys. Rev. C **58**, (1998) 1306.
211. P. Khaustov, et al., Phys. Rev. C **61**, (2000) 054603.
212. C.J. Batty, E. Friedman, and A. Gal, Phys. Lett. **B335**, (1994) 273.
213. J. Mareš, E. Friedman, A. Gal, and B.K. Jennings, Nucl. Phys. **A594**, (1995) 311.
214. H. Noumi, et al., Phys. Rev. Lett. **89**, (2002) 072301.
215. T. Harada and Y. Hirabayashi, Nucl. Phys. **A759**, (2005) 143.
216. E. Friedman and A. Gal, Phys. Rep. **452**, (2007) 89.
217. J. Schaffner and I.N. Mishustin, Phys. Rev. C **53**, (1996) 1416.
218. J. Schaffner, C.B. Dover, A. Gal, M. Hanauske, C. Greiner, D.J. Millener, and H. Stöcker, Ann. Phys. **235**, (1994) 35.
219. H. Dapo, B. J. Schaefer, and J. Wambach, Phys. Rec. C **81**, (2010) 035803.
220. H. Polinder, J. Haidenbauer, and U. G. Meißner, Nucl. Phys. **A779**, (2006) 244.
221. S. Hama, et al., Phys. Rev. C **41**, (1990) 2737.
222. E. D. Cooper, S. Hama, B. C. Clark, and R. L. Mercer, Phys. Rev. C **47**, (1993) 297.
223. M. Baldo, G.F. Burgio, and H.J. Schulze, Phys. Rev. C **58**, (1998) 3688.
224. Q. Li, Z. Li, E. Zhao, and R. K. Gupta, Phys. Rev. C **71**, (2005) 054907.
225. N.K. Glendenning, Phys. Rev. D **46**, (1992) 1274.
226. N.K. Glendenning, Phys. Rep. **342**, (2001) 393.
227. A. Chodos, R.L. Jaffe, K. Johnson, C.B. Thorn, and V.F. Weisskopf, Phys. Rev. D **9**, (1974) 3471.
228. U. Heinz, P.R. Subramanian, H. Stocker, and W. Greiner, J. Phys. G **12**, (1986) 1237.
229. M. Baldo, G.F. Burgio, and H.-J. Schulze, Phys. Rev. C **61**, (2000) 055801.
230. F. Sammarruca, Int. J. Mod. Phys. E **19**, (2010) 1259.
231. S. Köhler, Nucl. Phys. **A258**, (1976) 301.
232. E. Chabanat et al., Nucl. Phys. **627**, (1997) 710.
233. A. K. Dutta, J.-P. Arcoragi, J. M. Pearson, R. Behrman and E. Tondeur, Nucl. Phys. **A458**, (1986) 77.
234. F. Tondeur, A. K. Dutta, J. M. Pearson and R. Behrman, Nucl. Phys. **A470**, (1987) 93.
235. J. M. Pearson, Y. Aboussir, A. K. Dutta, R. C. Nayak, M. Farine and E. Tondeur, Nucl. Phys. **A528**, (1991) 1.
236. Y. Aboussir, J. M. Pearson, A. K. Dutta and F. Tondeur, Nucl. Phys. **A549**, (1992) 155.
237. M. Farine, J. M. Pearson and E. Tondeur, Nucl. Phys. **A615**, (1997) 135.
238. K. A. Brueckner and J. Dabrowski, Phys. Rev. **134**, (1964) B722.
239. J. Dabrowski and P. Haensel, Phys. Rev. C **7**, (1973) 916; Can. J. Phys. **52**, (1974) 1768.
240. D. W. L. Sprung and P. K. Banerjee, Nucl. Phys. **A168**, (1971) 273.
241. J. W. Negele, Phys. Rev. C **1**, (1970) 1260.

